



저작자표시-비영리-변경금지 2.0 대한민국

이용자는 아래의 조건을 따르는 경우에 한하여 자유롭게

- 이 저작물을 복제, 배포, 전송, 전시, 공연 및 방송할 수 있습니다.

다음과 같은 조건을 따라야 합니다:



저작자표시. 귀하는 원저작자를 표시하여야 합니다.



비영리. 귀하는 이 저작물을 영리 목적으로 이용할 수 없습니다.



변경금지. 귀하는 이 저작물을 개작, 변형 또는 가공할 수 없습니다.

- 귀하는, 이 저작물의 재이용이나 배포의 경우, 이 저작물에 적용된 이용허락조건을 명확하게 나타내어야 합니다.
- 저작권자로부터 별도의 허가를 받으면 이러한 조건들은 적용되지 않습니다.

저작권법에 따른 이용자의 권리는 위의 내용에 의하여 영향을 받지 않습니다.

이것은 [이용허락규약\(Legal Code\)](#)을 이해하기 쉽게 요약한 것입니다.

[Disclaimer](#)

A THESIS
FOR THE DEGREE OF MASTER OF SCIENCE

**Polyphenolic compounds isolated from marine algae;
potent inhibitors in SARS-CoV-2 proteases and cell entry**

D.P. Nagahawatta

Department of Marine Life Sciences
GRADUATE SCHOOL
JEJU NATIONAL UNIVERSITY

February, 2021

**Polyphenolic compounds isolated from marine algae; potent inhibitors
in SARS-CoV-2 proteases and cell entry**

D.P. Nagahawatta

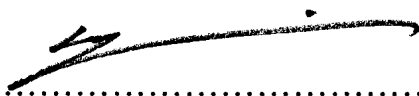
(Supervised by Professor You-Jin Jeon)

A thesis submitted in partial fulfilment of the requirement for the degree
of

Master of Science

February 2021

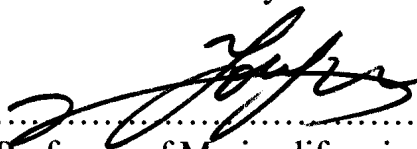
The thesis has been examined and approved by



.....
Thesis director, Seungheon Lee (PhD), Professor of Marine life sciences,
Jeju National University



.....
Gi-Young Kim (PhD), Professor of Marine life sciences, Jeju National
University



.....
You-Jin Jeon (PhD), Professor of Marine life sciences, Jeju National
University

2021/02

Date

Department of Marine Life Sciences

GRADUATE SCHOOL

JEJU NATIONAL UNIVERSITY



Contents

Summary	iii
List of figures	v
List of Tables	viii
Polyphenolic compounds isolated from marine algae; potent inhibitors in SARS-CoV-2 proteases and cell entry	1
1. Introduction.....	2
2. Methods and Materials.....	8
2.1 Chemicals and reagents.....	8
2.2 Preparation of Receptors	8
2.3. Preparation of ligands	9
2.4 Molecular docking	11
2.5 Sample collection and extraction	11
2.6 Isolation of Ishophloroglucin A	12
2.7 Isolation of Dieckol.....	14
2.8 Isolation of Eckmaxol	15
2.9 3CL ^{pro} <i>in-vitro</i> cleavage inhibition assay	17
2.10 PL ^{pro} <i>in-vitro</i> cleavage inhibition assay	17
2.11 Inhibition assay in binding of ACE-2 receptor and SARS-CoV-2 spike protein	18

2.12 Statistical analysis	19
3. Results.....	20
3.1 Receptor and ligand preparation	20
3.1.1. Structure of ACE-2 receptor protein preparation	20
3.1.2. Structure of 3CL ^{pro} receptor protein preparation.....	22
3.1.3 Structure of PL ^{pro} receptor protein preparation	24
3.1.4 Ligand preparation.....	26
3.2 Molecular docking	28
3.2.1. ACE-2 enzyme	32
3.2.2. 3CL ^{pro} enzyme	34
3.2.3. PL ^{pro} enzyme	37
3.3 In-vitro inhibition of marine algal compounds	40
4. Discussion.....	43
5. Conclusions.....	46
Acknowledgment.....	47
References.....	48

Summary

The recent pandemic of coronavirus disease 2019 (COVID-19) caused by SARS-CoV-2 has raised global health concern. The identified coronavirus expressed significant differences from the other respiratory pathogens such as severe acute respiratory coronavirus (SARS-CoV), Middle East respiratory syndrome coronavirus (MERS-CoV), influenza, adenovirus, and avian influenza. The actual infection mechanism of SARS-CoV-2 is still unrevealed 100% such as why the virus has selected humans as a principal host and how to escape the innate immune system. However, the viral entry mechanism has been identified and it invades the human body through the respiratory system using respiratory droplets via sneeze and cough.

SARS-CoV-2 consists of protein capsid covered by glycoprotein with anchored spike proteins. These spike proteins initiate the viral entry into target cells. Entry of SARS-CoV-2 into the host cell is an important factor to determine the infectivity and pathogenesis. SARS-CoV-2 spike protein initially binds to the cell surface receptor called angiotensin-converting enzyme 2 (ACE-2) and this is known as viral attachment, subsequently, enter to endosome and finally viral membrane fuse with lysosomal membrane. Thus, if some particular compound has a potential to interfere with the interaction of ACE-2: RBD of spike protein of SARS-CoV-2, it has a potential for using against SARS-CoV-2 cell entry mechanism.

Among the excellent drug targets of SARS-CoV-2 are its proteases (NSP 3 and NSP 5) that play vital role in polyprotein processing giving rise to functional non-structural proteins, essential for viral replication and survival. Nsp5 (also known as 3CL^{pro}) hydrolyses replicase polyprotein (1ab) at eleven different sites. The resulted products are important for survival and replication of virus in host cell. The papain-like

protease (PL^{pro}) cleaves the viral polyprotein, and reverses inflammatory ubiquitin and anti-viral ubiquitin-like ISG15 protein modifications. Therefore, Drugs that target SARS-CoV-2 PL^{pro} may hence be effective as treatments or prophylaxis for covid-19, reducing viral load and reinstating innate immune responses.

The SARS-CoV-2 infection and replication is a complex mechanism and this aspect suggests that a COVID-19 therapy by a multi-targeting approach is the right way. Bioactive components from marine algae have provided new insight to the natural product research. The present study aims to inhibit SARS-CoV-2 through 3CL^{pro}, PL^{pro}, and SARS-CoV-2 cell entry mechanism by natural products isolated from marine algae. Molecular docking was utilized for the initial screening of selected natural products based on the 3CL^{pro}, PL^{pro}, and ACE-2 protein structures. Moreover, the resulted compounds were isolated and used for biological assays for further confirmation of the inhibition activity. To the best of our knowledge, this is the first report concerning the assessment of marine natural products on 3CL^{pro}, PL^{pro}, and ACE-2 of SARS-CoV-2.

Keywords: SARS-CoV-2; 3CL^{pro}; PL^{pro}; ACE-2; Marine algae, Molecular docking

List of figures

Fig. 1. Cell entry mechanism and spike protein structure. a) SARS-CoV-2 cell entry mechanism, b) SARS-CoV spike protein structure.	5
Fig. 2 Chemical structures of ligand.....	10
Fig. 3. a) Extraction and fractionation of <i>Ishige okamurae</i> . b) High performance Liquid chromatography (HPLC) analysis of Ishoploroglucin A	13
Fig. 4. a) Extraction and fractionation of <i>Ecklonia cava</i> . b) High Performance Liquid Chromatography (HPLC) analysis of Dieckol.....	14
Fig. 5. a) Extraction and fractionation of <i>Ecklonia maxima</i> . b) High Performance Liquid Chromatography (HPLC) analysis of Eckmaxol.	16
Fig. 6. a) Surface representation ACE-2: RBD of SARS-CoV-2 spike protein complex ACE-2. ACE-2 receptor protein is in yellow colour and RBD of SARS-CoV-2 is in red colour. b) Cartoon representation of ACE-2: RBD of SARS-CoV-2 spike protein complex. ACE-2 receptor protein is in yellow color and RBD of SARS-CoV-2 is in red color. c) Prepared active site of ACE-2.	21
Fig. 7. a) a) Surface representation 3CL ^{pro} and N3 inhibitor ligand complex 3CL ^{pro} receptor protein is in yellow color and N3 inhibitor in red color. b) Cartoon representation of 3CL ^{pro} and N3 inhibitor ligand complex. 3CL ^{pro} receptor protein is in yellow color and N3 inhibitor is in red color. c) 2D representation of ligand interaction between 3CL ^{pro} and N3 inhibitor. d) 3D representation of ligand interaction between 3CL ^{pro} and N3 inhibitor. e) Prepared active site of 3CL ^{pro}	23
Fig. 8. a) Surface representation PL ^{pro} and GRL0617 inhibitor ligand complex 3CL ^{pro} receptor protein is in yellow color and GRL0617 inhibitor in red color. b) Cartoon representation of PL ^{pro} and GRL0617 inhibitor ligand complex. PL ^{pro} receptor protein is	

in yellow color and GRL0617 inhibitor is in red color. c) 2D representation of ligand interaction between PL^{pro} and GRL0617 inhibitor. d) 3D representation of ligand interaction between PL^{pro} and GRL0617 inhibitor. e) Prepared active site of PL^{pro}.25

Fig. 9. Three-dimensional structures of prepared ligand using Discovery studio.27

Fig. 10. a) 3D representation of docking pose of IPA with ACE-2. b) Cartoon representation of docking pose of IPA with ACE-2. c) 2D representation of Ligand interaction of IPA with ACE-2. d) 3D representation of Ligand interaction of IPA with ACE-2.32

Fig. 11. a) 3D representation of docking pose of Eckmaxol with ACE-2. b) Cartoon representation of docking pose of Eckmaxol with ACE-2. c) 2D representation of Ligand interaction of Eckmaxol with ACE-2. d) 3D representation of Ligand interaction of Eckmaxol with ACE-2.33

Fig. 12. a) 3D representation of docking pose of IPA with 3CL^{pro}. b) Cartoon representation of docking pose of IPA with 3CL^{pro}. c) 2D representation of Ligand interaction of IPA with 3CL^{pro}. d) 3D representation of Ligand interaction of IPA with 3CL^{pro}.34

Fig. 13. a) 3D representation of docking pose of Dieckol with 3CL^{pro}. b) Cartoon representation of docking pose of Dieckol with 3CL^{pro}. c) 2D representation of Ligand interaction of Dieckol with 3CL^{pro}. d) 3D representation of Ligand interaction of Dieckol with 3CL^{pro}.35

Fig. 14. a) 3D representation of docking pose of Eckmaxol with 3CL^{pro}. b) Cartoon representation of docking pose of Eckmaxol with 3CL^{pro}. c) 2D representation of Ligand interaction of Eckmaxol with 3CL^{pro}. d) 3D representation of Ligand interaction of Eckmaxol with 3CL^{pro}.36

Fig. 15. a) 3D representation of docking pose of IPA with PL ^{pro} . b) Cartoon representation of docking pose of IPA with PL ^{pro} . c) 2D representation of Ligand interaction of IPA with PL ^{pro} . d) 3D representation of Ligand interaction of IPA with PL ^{pro}	37
Fig. 16. a) 3D representation of docking pose of Dieckol with PL ^{pro} . b) Cartoon representation of docking pose of Dieckol with PL ^{pro} . c) 2D representation of Ligand interaction of Dieckol with PL ^{pro} . d) 3D representation of Ligand interaction of Dieckol with PL ^{pro}	38
Fig. 17. a) 3D representation of docking pose of Eckmaxol with PL ^{pro} . b) Cartoon representation of docking pose of Eckmaxol with PL ^{pro} . c) 2D representation of Ligand interaction of Eckmaxol with PL ^{pro} . d) 3D representation of Ligand interaction of Eckmaxol with PL ^{pro}	39
Fig. 18. <i>In-vitro</i> inhibition assay of the interaction between ACE-2: SARS-CoV-2 a) Ishophloroglucin A and b) Eckmaxol.	41
Fig. 19. <i>In-vitro</i> inhibition assay of 3CL ^{pro} a) Ishophloroglucin A and b) Dieckol, and c) Eckmaxol.	41
Fig. 20. <i>In-vitro</i> inhibition assay of PL ^{pro} a) Ishophloroglucin A, b) Dieckol, and c) Eckmaxol.	42

List of Tables

Table 1. The cDocke interaction energies and free binding energies (Kcal/ mol) of selected ligands from marine algae with ACE-2 receptor protein.....	29
Table 2. The cDocke interaction enrgies and free binding enrgies (Kcal/ mol) of selected ligands from marine algae with 3CL ^{pro} receptor protein.	30
Table 3. The cDocke interaction energies and free binding energies (Kcal/ mol) of selected ligands from marine algae with PL ^{pro} receptor protein.....	31
Table 4. Inhibitory activity of isolated compounds on the cell free cleavage of 3CL ^{pro} , PL ^{pro} and interactions of ACE-2: SARS-CoV-2 spike protein.	40

**Polyphenolic compounds isolated from marine algae;
potent inhibitors in SARS-CoV-2 proteases and cell entry**

1. Introduction

An unknown series of pneumonia cases were identified in December 2019 emerged in Wuhan, Hubei province, China. According to the world health organization (WHO) country office of China, the infected clusters were initially reported on 31st of December 2019. The new type of coronavirus was identified by the Chinese authority on 7th January 2020 that causes a new infectious respiratory disease called severe acute respiratory syndrome coronavirus 2 (SARS-CoV-2). The identified coronavirus expressed significant differences from the other respiratory pathogens such as severe acute respiratory coronavirus (SARS-CoV) and Middle East respiratory syndrome coronavirus (MERS-CoV), influenza, adenovirus, avian influenza. The information conveyed by Chinese authorities to WHO on 11th and 12th January 2020 revealed 41 infected cases with 7 serious situations and 1 death. The patient who died due to SARS-CoV-2 infections was suffered from other underlying health conditions (<https://www.who.int/csr/don/12-january-2020-novel-coronavirus-china/en/>). The origin of the SARS-CoV-2 is still unclear, but RaTG13, the coronavirus isolated from bats expressed close genetic similarity with SARS-CoV-2. Therefore, bats are considered as the origin of this [1]. However, the transmission mechanism of the virus from bat to human is still unclear.

Coronaviruses that belong to the family *Coronaviridae* are enveloped non-segmented, positive-sense, single-stranded RNA viruses, and in the order of *Nidovirales* [2]. The mentioned viruses widely infect humans and other mammals. According to the previous reports, SARS-CoV and MERS-CoV caused a pandemic situation in the world and was responsible for around 10 000 cumulative cases and the mortality rate was 10% and 37% respectively [3]. SARS was revealed in 2002 in Guangdong province, China and it was responsible for 8096 infected cases and 774 deaths [4]. Furthermore, Chinese horseshoe

bats were identified as natural reservoir hosts for SARS-CoV [5]. The SARS-CoV was controlled using conventional methods such as travel restrictions and isolation of patients. The mentioned novel disease SARS-CoV-2 which identified from Wuhan had linked with Hunan seafood market and therefore, expertise believes that SARS-CoV-2 was infected from animal to human and it was spread rapidly from human to human [6].

The actual infection mechanism of SARS-CoV-2 is still unrevealed such as why the virus has selected humans as a principal host and how it escapes the innate immune system. Moreover, the interaction between human Toll-like receptor and (TLR) and viral antigens and the mechanism of pro-inflammatory cytokine production and its effect on the important human organs are not fully uncovered. However, the viral entry mechanism has been identified and it invades the human body through the respiratory system using respiratory droplets via sneeze and cough [7]. SARS-CoV-2 consists of protein capsid covered by glycoprotein with anchored spike proteins. These spike proteins initiate the viral entry into target cells. Entry of SARS-CoV-2 into the host cell is an important factor to determine the infectivity and pathogenesis [8]. Therefore, it is a key target for host immune monitoring and human intervention strategies [9]. SARS-CoV-2 spike protein initially binds to the cell surface receptor called angiotensin-converting enzyme 2 (ACE-2) and this is known as viral attachment, subsequently, it enters into endosome and finally viral membrane fuse with lysosomal membrane (Fig. 1a). SARS-CoV spike protein is present as a trimer in the mature virus. Furthermore, this trimer consists of 3 receptor binding S1 heads and S2 stalk. The S1 contains a receptor-binding domain (RBD) that switches between two positions. The lying down position is used for immune evasion and the standing-up position for binding with host receptor ACE-2 (Fig. 1b) [10]. Previous studies provide solid shreds of evidence such as crystal structures of SARS-CoV RBD from different strains in complex with ACE-2 from different hosts. According to these

structures, SARS-CoV RBD consists of receptor binding motif (RBM), and RBM constructs a contact with ACE-2. The ACE-2 receptor consists of 2 essential virus binding hot spots on its surface and SARS-CoV RBM regulates its infectivity through these hot spots [11-13]. As mentioned before, the SARS-CoV spike protein consists of S1 and S2 subunits. This S1 unit facilitates the binding with ACE-2. However, the entry mechanism requires S protein priming. Therefore, cellular serine proteases such as TMPRSS2 and TMPRSS11D cleave the spike protein at the S1/S2 and S1 sites. This cleavage allows the fusion between spike protein and cellular membranes[14]. SARS-CoV-2 spike protein showed 76% to 78% sequence similarity for whole protein, 73% to 76% for RBD, and 50% to 53% for the RBM with SARS-CoV. Moreover, the similarity of spike protein between SARS-CoV and SARS-CoV-2 provides the insight to share the same host receptor ACE-2. Further, RBM of SARS-CoV-2 does not contain any insertion or deletion and when considering about 14 residues of RBD that provide contact with ACE-2 receptor, 9 fully conserved residues, and 4 partially conserved residues can be identified between the mentioned two strains [15]. Hence, the inhibition of binding between the RBD of SARS-CoV-2 and ACE-2 receptor can be identified as a potential way to inhibit the SARS-CoV-2 infection.

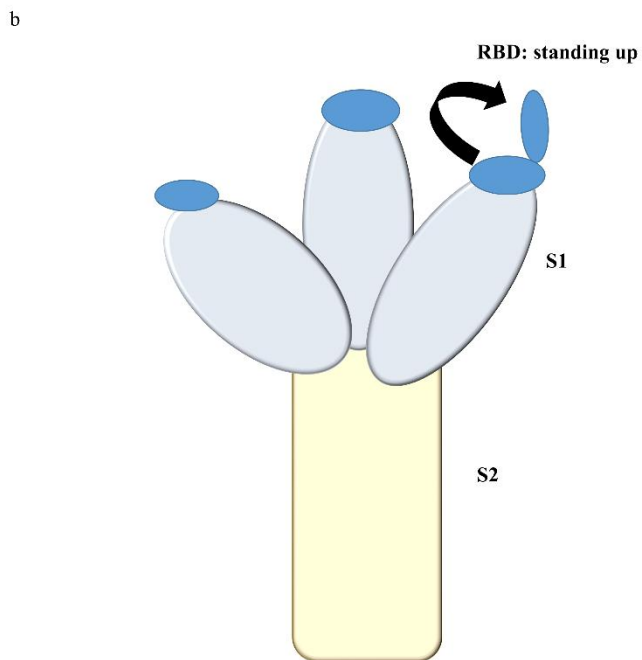
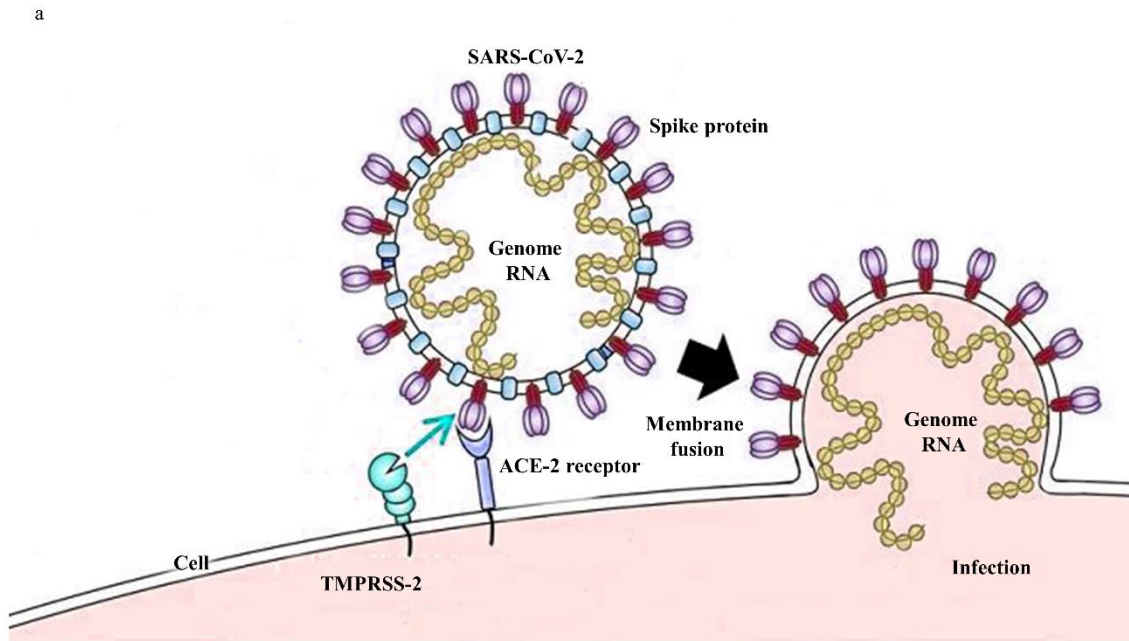


Fig. 1. Cell entry mechanism and spike protein structure. a) SARS-CoV-2 cell entry mechanism, b) SARS-CoV spike protein structure.

Coronaviruses contain 26 to 32kb length RNA viral genome. The newly sequenced SARS-CoV-2 genome was submitted in the NCBI genome database under accession number NC_045512.2 and the size was ~29.9kb [16]. SARS-CoV-2 consists of 13 to 15 open reading frames (ORFs) including 12 functioning ORFs. The ORFs are arranged as protease, replicase, and main structural proteins including spike, envelop, membrane, and nucleocapsid proteins. When considering the whole genome of SARS-CoV-2, it encodes for polyprotein which consist of ~7096 residues. It contains many structural and non-structural proteins (NSPs) and ORF1a and ORF1b that encodes for non-structural proteins are mainly responsible for the nucleotide content of the genome. ORF 1a and 1b encode the polyprotein pp1a and pp1b respectively and gene 1b employs the ribosomal frameshift mechanism to encode pp1ab. The virally encoded proteases cleave these polyproteins and produce 16 NSPs and the rest of the genome responsible for structural proteins. These proteins play a pivotal role in viral entry fusion, replication, and survival in host cells. Thus, these gene products are considered as the main drug or vaccine targets [17]. Polyprotein processing is mainly conducted by 3-chymotrypsin-like protease (3CL^{pro}) and papain-like protease (PL^{pro}). The polyprotein is cleaved at 11 distinct sites by 3CL^{pro}. This leads to the production of important NSPs which are important in viral replication [18]. 3CL^{pro} plays a key role in SARS-CoV-2 replication in the host cell. According to the previous studies, high-throughput studies and structure-based activity analysis confirmed the value of the potential inhibitors for the activity of 3CL^{pro} against SARS-CoV and MERS-CoV which successfully inhibited the virus replication [19-21]. Therefore, 3CL^{pro} of SARS-CoV-2 is considered as a potential drug candidate. PL^{pro} of SARS-CoV and SARS-CoV-2 express 83% sequence identity and diverge from MERS-CoV. However, the host substrate preference of PL^{pro} is the difference between these two strains. Further, PL^{pro} of SARS-CoV-2 cleaves the ubiquitin-like interferon-stimulated

gene 15 protein (ISG15) and PL^{pro} of SARS-CoV predominantly targets the ubiquitin chain [22]. ISG15 regulates various cellular signalling pathways and host immune responses. Therefore, 3CL^{pro} and PL^{pro} are identified as potential drug targets to inhibit SARS-CoV-2.

Marine algae confront extreme environmental conditions and their metabolism consists of a biochemical process to absorb nutrients and convert them into materials that are important for survival from these particular environmental conditions [23]. These accumulated defence metabolites express elevated potential to develop new therapeutic agents [24].

The present study aims to inhibit SARS-CoV-2 through 3CL^{pro}, PL^{pro}, and ACE-2: SARS-CoV-2 spike protein binding using natural products isolated from marine algae. Molecular docking was utilized for the initial screening of selected natural products based on the 3CL^{pro}, PL^{pro}, and ACE-2 protein structures. Moreover, the resulted compounds were isolated and used for biological assays for further confirmation of the inhibition activity. To the best of our knowledge, this is the first report concerning the assessment of marine natural products on 3CL^{pro}, PL^{pro}, and ACE-2 of SARS-CoV-2.

2. Methods and Materials

2.1 Chemicals and reagents

Dimethylsulfoxide (DMSO) and All the organic solvents (HPLC grade) used in the experiments were purchased from Sigma-Aldrich (St Louis, MO, USA). The in-vitro inhibition assay kits for ACE-2: SARS-CoV-2 spike, 3CL^{pro}, and PL^{pro} were purchased from AMSBIO company (Madrid, Spain).

2.2 Preparation of Receptors

The protein Data Bank (PDB) (<http://www.pdb.org>) was used to obtain crystal structures of 3CL^{pro}, PL^{pro}, and ACE-2 under PDB ID: 6LU7, 7CMD, and 6LZG respectively. The molecular docking studies were conducted using Discovery studio (DS Client v18.1.100.18065). Briefly, crystal structure of each protein was downloaded from the PDB and open in the DS. The water molecules and heteroatoms were removed and The “Clean protein” tool was used to correct minor problems such as, missing-side chain atoms which were added in an extended confirmation.

The “Prepare protein” tool was utilized to solve most common problems such as removing of alternate conformations, removing of heteroatoms, hydrogens addition, and correcting of missing or incorrectly specified residues. The energy minimization of target receptor proteins was performed using “Protein minimization” tool. DS provides three options to prepare the binding site of the receptor protein, “based on the PDB site records”, “from receptor cavities”, and “form current selection”. Present study used the last tool based on the available ligands of the crystal structures and previously published data. The crystal structure of 3CL^{pro} was available in the PDB as a complex with an inhibitor called Michael acceptor inhibitor or N3 inhibitor. The binding site of 3CL^{pro}

was determined based on the mentioned inhibitor and previous studies [25]. PL^{pro} was available in the PDB as a complex with an inhibitor GRL0617. Therefore, the binding site of PL^{pro} was determined using GRL0617 and previous studies[26]. ACE-2 was available in PDB as a complex with SARS-CoV-2 spike protein. The chain B SARS-CoV-2 spike protein was removed and the binding site was determined based on the previous studies [27]. Briefly, the binding site was prepared as a grid in the ligand binding site of the crystal structure and the prepared binding sites of the target proteins was identified itself by specifying a sphere of given radius located in the active site. The geometric center of the ligand in crystal structure was used as a center of the sphere. Python-enhanced molecular graphics tool (PyMOL, version 2.4.1) was used to calculate the root-mean-square deviation of atomic position (RMSD) value of the prepared 3CL^{pro} and raw 3CL^{pro} to determine any significant difference between them.

2.3. Preparation of ligands

The ligands were 16 compounds from marine algae. The 3D structure of each compound was generated and hydrogen atoms were added. The energy of the ligand was minimized using “Clean geometry” tool and apply CHARMM force field. The final ligand structure generated by “Prepare ligand” tool was optimized using DS ligand optimization. The summary of the ligands that used in this study were shown in Fig. 2. The ligands that selected for validation were 16 compounds from marine algae.

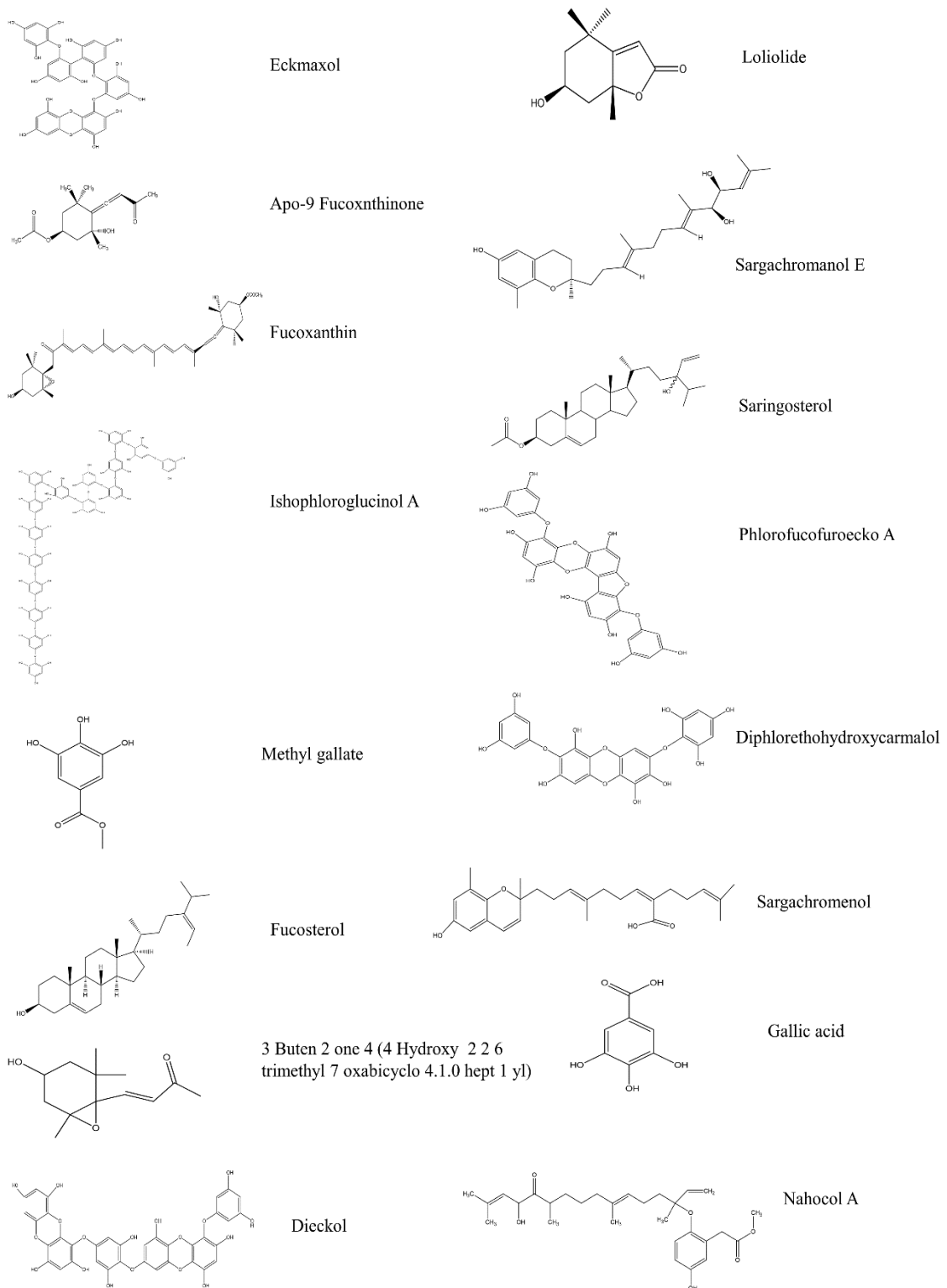


Fig. 2. Chemical structures of ligand.

2.4 Molecular docking

Docking of the selected ligands with prepared proteins was performed using DS. The crystal structure of 3CL^{pro} bound with N3 inhibitor and PL^{pro} bound with GR10617 were reproduced and the RMSD value between the raw crystal structure and docking results were calculated to confirm the accuracy of the process. Initially, Flexible docking experiments were performed using the 3D crystal structure of 3CL^{pro}, PL^{pro}, and ACE-2. Flexible docking is a fully automated workflow. The flexible docking protocol allows for receptor flexibility during docking of flexible ligands. The side chains of specified amino acids in target receptor protein are allowed to move during docking. Moreover, receptor was adapted to different ligands in an induced-fit model. Therefore, flexible docking was performed to determine the suitable orientation of ligand in the active site of each receptor protein. The obtained results from the flexible docking were used to calculate the binding energy between each ligand and receptor proteins using CHARMM based energy. The free energy of the complex, the ligand, and the receptor was used to calculate the free energy of binding.

$$\text{Energy binding} = \text{Energy Complex} - (\text{Energy Ligand} + \text{Energy Receptor})$$

The three ligands were selected for biological assays based on the results of molecular docking.

2.5 Sample collection and extraction

Brown algae *Ishige okamurae* (IO), *Ecklonia cava* (EC) were collected from the coastal area of Seongsan, Jeju, South Korea in February 2019. *Ecklonia maxima* (EM) was collected from the coastal area of Cape town, South Africa in 2019 February. Samples

were washed 4 times immediately after harvest with running water for removing salt, attached sand, and epiphytes. The washed seaweeds were stored under $-70\text{ }^{\circ}\text{C}$. The frozen seaweeds were lyophilized using freeze dryer and dried seaweeds were ground into powder. Sample extraction was initiated using 70% ethanol for three times under room temperature. The subsequent solution was evaporated using rotary evaporator and obtained resulted powder of ethanol extract of IO (IOE), EC (ECE), and EM (EME). IOE, ECE, and EME were dissolved in deionized water and successfully fractionated using n-hexane, chloroform, ethyl acetate and butanol respectively. The each resulted fractions were evaporated and ethyl acetate fraction of IO (IOEA), EC (ECEA), and EM (EMEA) were utilized to isolate the interested compounds. The centrifugal partition chromatography (CPC 240, Tokyo, Japan) and the ODS cartridge in FlashPrep system (C-850 FlashPrep, BUCHI, Swisterland) was utilized to further separation of IOEA, ECEA, and EMEA.

2.6 Isolation of Ishophloroglucin A

The centrifugal partition chromatography (CPC 240, Tokyo, Japan) was utilized to isolate IPA. The rotor volume was 1L. The method was continued in a two phase solvent system which consist of n-hexane: ethyl acetate: methanol: water with 1: 9: 4.5: 6.5 v/v ratio. These solvents were thoroughly mixed and equilibrated in a separatory funnel. The upper organic phase act as a stationary phase and lower aqueous phase act as a mobile phase. The CPC instrument was conditioned until it reached the hydrostatic equilibrium and the 500mg of IOEA was dissolved in 6ml of 1:1 v/v water: methanol of CPC solvent system and injected using isocratic pump (Kromaton). The effluent was monitored at 230 nm and fractions were collected into test tubes using fraction collector (3min for each tube). All collected fractions from the same compounds were pooled for continuing further

purification. The high performance liquid chromatography (HPLC) system (Milford, Massachusetts, USA) equipped with PDA detector was used to further purification. The semi-preparative column HPLC column YMC-Pack ODS-A 10 mm × 250 mm, 5 μm (YMC Co., Ltd, Kyoto, Japan) was used with an isocratic solvent mode (32% acetonitrile with 1% formic acid) and flow rate was 2 ml/ min [28] (Fig. 3)

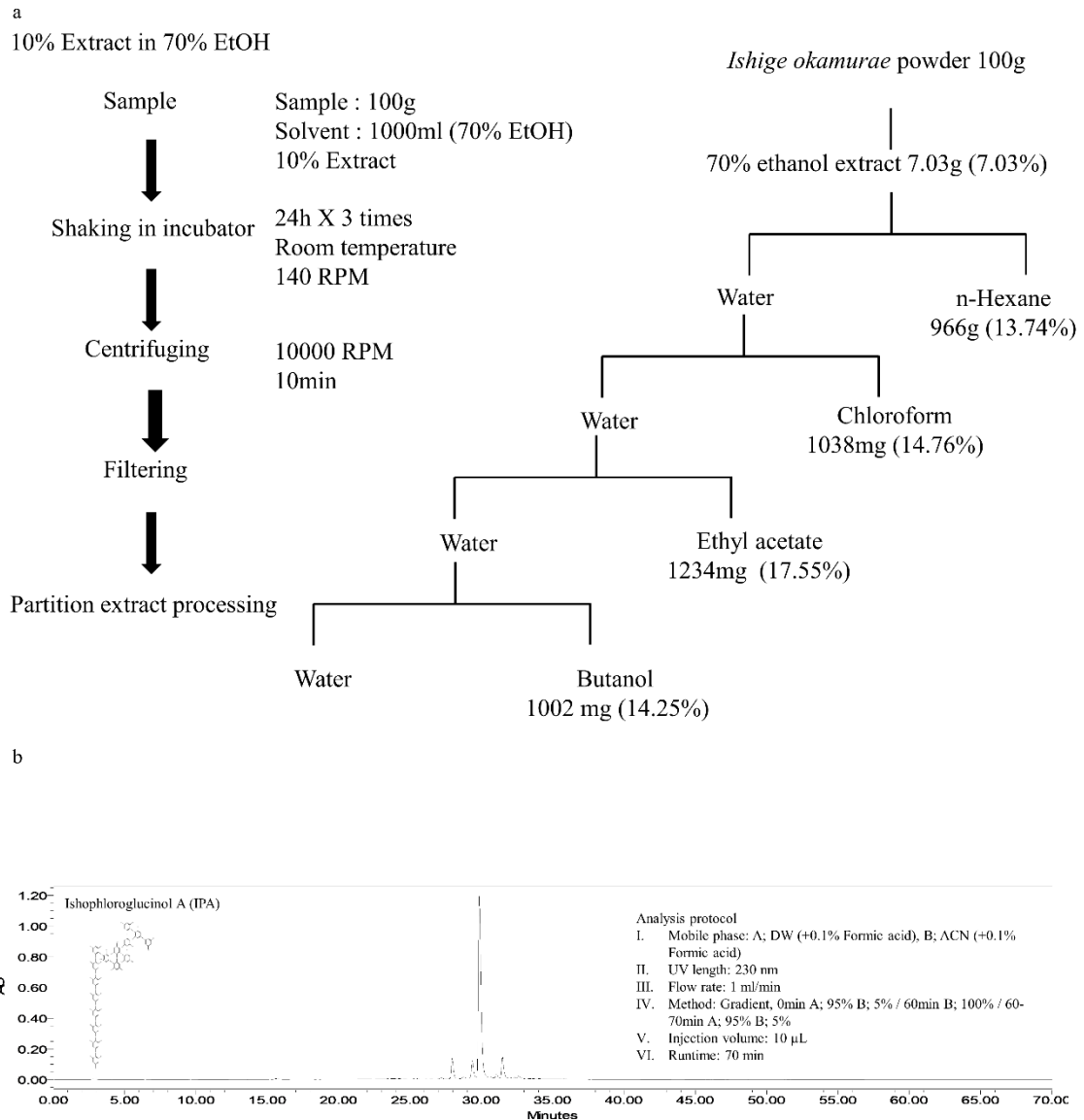


Fig. 3. a) Extraction and fractionation of *Ishige okamurae*. b) High performance Liquid chromatography (HPLC) analysis of Ishophloroglucinol A

2.7 Isolation of Dieckol

The Dieckol was isolated from ECEA using ODS cartridge in Flashprep system (C-850 FlashPrep, BUCHI, Swisterland) equipped with PDA and ELSD detectors. The packing PREP C18, 55-105 μm , 125 °A (waters, Milford, USA) column was used with 20ml/min flow rate. The mobile phase was consisted of water and acetonitrile with a gradient method (0 min 90:10 v/v, 0-12 min 90:10 v/v, 12-36 min 85:15 v/v, 36-68 min 80:20 v/v, 68-80 min 0:100 v/v). The fractions were collected based on the results at 230 nm (Fig. 4).

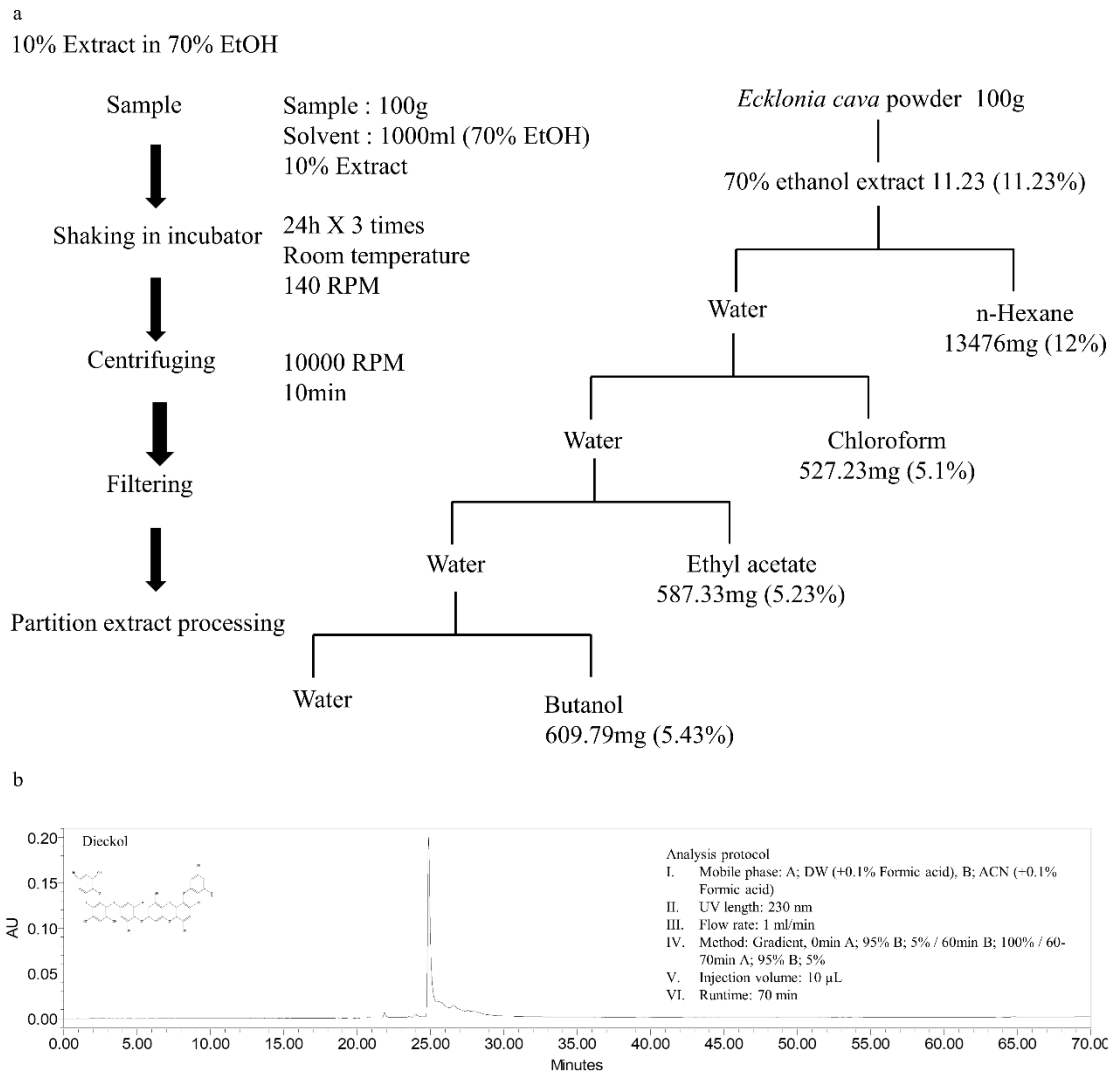


Fig. 4. a) Extraction and fractionation of *Ecklonia cava*. b) High Performance Liquid Chromatography (HPLC) analysis of Dieckol.

2.8 Isolation of Eckmaxol

The Eckmaxol was isolated from EMEA using the centrifugal partition chromatography (CPC 240, Tokyo, Japan) method comprising of n-hexane: ethyl acetate: methanol: water with 3: 7: 4: 6: v/v ratio. The mentioned solvents were vigorously mixed and equilibrated for separating two phases under room temperature. The upper organic phase was used as a stationary phase and lower aqueous phase was used as a mobile phase. The organic stationary phase was filled into CPC column and rotated at 1000 rpm and the aqueous mobile phase was pumped into the column in a descending mode at flow rate of 2ml/min. The hydrodynamic equilibrium was maintained before injecting the sample and 500mg of EMEA that dissolved in 6ml of 1:1 v/v water: methanol was injected through the injection valve. The automatic fraction collector was utilized to collect fractions (6ml for each tube) under 230nm UV detection range. The HPLC system (Milford, Massachusetts, USA) equipped with PDA detector was used for further purification. YMC-Pack ODS-A 10 mm × 250 mm, 5 μm column (YMC Co., Ltd, Kyoto, Japan) with acetonitrile + 0.1% formic acid and deionized water + 0.1% formic acid was used as a mobile phase and flow rate was 2 ml/ min [29] (Fig. 5).

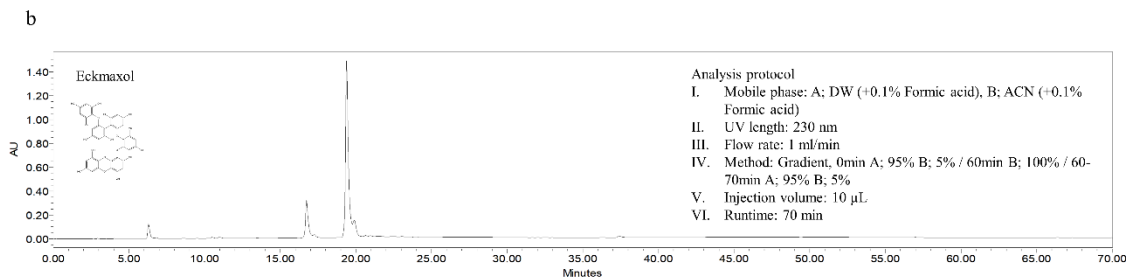
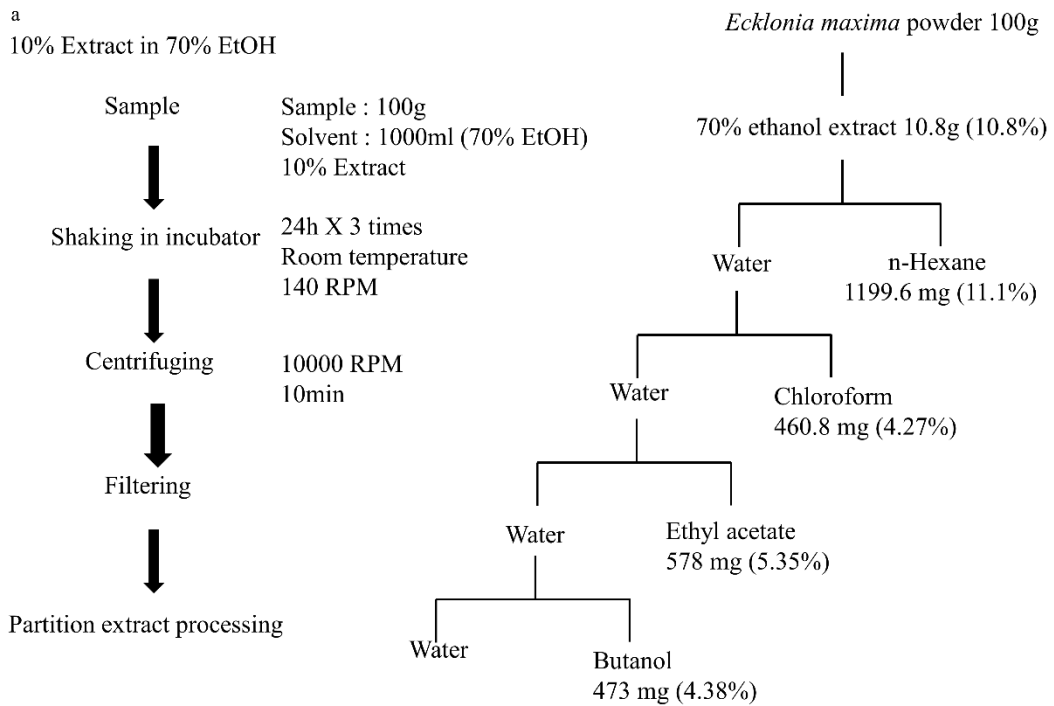


Fig. 5. a) Extraction and fractionation of *Ecklonia maxima*. b) High Performance Liquid Chromatography (HPLC) analysis of Eckmaxol.

2.9 3CL^{pro} *in-vitro* cleavage inhibition assay

The inhibitory activity of interested compounds was measured using “3CL protease (SARS-CoV-2)” assay kit (AMSBIO, Madrid, Spain). The interested compounds were dissolved in Dimethyl sulfoxide (DMSO) and diluted into assay buffer available with kit. The final DMSO concentration of the highest concentration of each compound used in the assay was less than 1%. IPA, Dieckol, and Eckmaxol were incubated with 120 ng of 3CL^{pro} enzyme for 30 min under room temperature with slow shaking. The broad spectrum antiviral medication GC376 was used as a test inhibitor in the assay and 50 μM of fluorogenic substrate was added to each well. The experiment was performed in 96 well plate. The positive control was the well that contained only 3CL^{pro} enzyme and fluorogenic substrate used to measure the enzyme activity and blank well contain only substrate. The enhanced fluorescence emission due to substrate cleavage was monitored at excitation (360 nm) and emission (460 nm) using Synergy HTX multi-mode microplate reader (Vermont, USA)

The IC₅₀ value of each compounds were calculated and the experimental data were fit to a logistic curve with below mentioned equation.

$$\text{Enzyme activity \%} = [S - B] / [P - B] * 100\%$$

“B” is florescence of control (substrate and assay buffer), “P” is the florescence of positive control (substrate and enzyme), and “S” is the florescence of the tested sample.

2.10 PL^{pro} *in-vitro* cleavage inhibition assay

PL^{pro} enzyme inhibition activity of isolated compounds were evaluated using “Papain-like protease (SARS-CoV-2)” assay kit (AMSBIO, Madrid, Spain). The isolated compounds were dissolved in DMSO and diluted into assay buffer with less than 1%

DMSO concentration in assay buffer. The diluted concentrations of IPA, Dieckol, and Eckmaxol were treated into each well that contain 1.2 ng of PL^{pro} enzyme and incubated for 30 min with slow shaking under room temperature. Blank well was treated with only 25 μM fluorogenic substrate and positive control well contained only PL^{pro} enzyme and fluorogenic substrate. The experiment was performed in 96 well plate and positive control well was used to evaluate the enzyme activity. The enhanced fluorescence emission due to substrate cleavage was monitored at excitation (360 nm) and emission (460 nm) using Synergy HTX multi-mode microplate reader (Vermont, USA) and The IC₅₀ value of each compounds were calculated and the experimental data were fit to a logistic curve with below mentioned equation.

$$\text{Enzyme activity \%} = [S - B] / [P - B] * 100\%$$

“B” is florescence of control (substrate and assay buffer), “P” is the florescence of positive control (substrate and enzyme), and “S” is the fluorescence of the tested sample.

2.11 Inhibition assay in binding of ACE-2 receptor and SARS-CoV-2 spike protein

The inhibitory potential of isolated compounds in binding of ACE-2: SARS-CoV-2 spike protein was evaluated using ACE-2: SARS-CoV-2 inhibitor screening assay kit (AMSBIO, Madrid, Spain). Briefly, 50 ng of his-tagged ACE-2 protein was added to the nickel-coated well and blocked using blocking buffer. The isolated compounds IPA, Eckmaxol, Dieckol, were added to the each well except blank and positive control. Finally, 20 ng of spike protein was added to each well except blank and incubated 1h under room temperature with slow shaking. The Fc-tagged spike protein was detected using HRP-labelled anti-Mouse-Fc. The luminescence which emit due to chemical reaction was detected using Synergy HTX multi-mode microplate reader (Vermont,

USA). The detection of chemiluminescence was performed without selected wavelength, because this method used emission photometry. The enhanced chemiluminescence was measured using Synergy HTX multi-mode microplate reader (Vermont, USA) The IC₅₀ value of each compounds were calculated and the experimental data were fit to a logistic curve with below mentioned equation.

$$\text{Enzyme activity \%} = [S - B] / [P - B] * 100\%$$

“B” is florescence of control (substrate and assay buffer), “P” is the florescence of positive control (substrate and enzyme), and “S” is the fluorescence of the tested sample.

2.12 Statistical analysis

All compounds were examined in the set of triplicate experiments. IC₅₀ (50% inhibitory concentration) values of compounds represent the concentration that caused 50% enzyme activity loss. Using a minimum of three samples, standard deviation was calculated in all experiments. The inhibition mechanism of the compounds was determined by comparing the statistical results, including the Akaike’s information criterion values, of different inhibition models and selecting the one with the best fit [30].

3. Results

3.1 Receptor and ligand preparation

3.1.1. Structure of ACE-2 receptor protein preparation

The X-ray crystallography of the human ACE-2 receptor (PDB ID 6LZG) was obtained from PDB. The present structure was available as a complex with RBD of SARS-CoV-2 spike protein at a high resolution of 2.5 Å. The total structure weight was 93.5 kDa (Fig. 6a). The RBD of SARS-CoV-2 spike protein was bound to the human ACE-2 receptor through SER19, GLN24, PHE28, ASP30, LYS31, HIS34, ASP38, TYR41, GLN42, LEU79, MET82, TYR83, LYS353, ASP355 (Fig. 6b). The active site was prepared using these residues and the binding site sphere was prepared with a 15 Å radius. The prepared ACE-2 was superimposed with the original ACE-2 available in PDB using PyMOL and the calculated RMSD value was 0.25 (Fig. 6c).

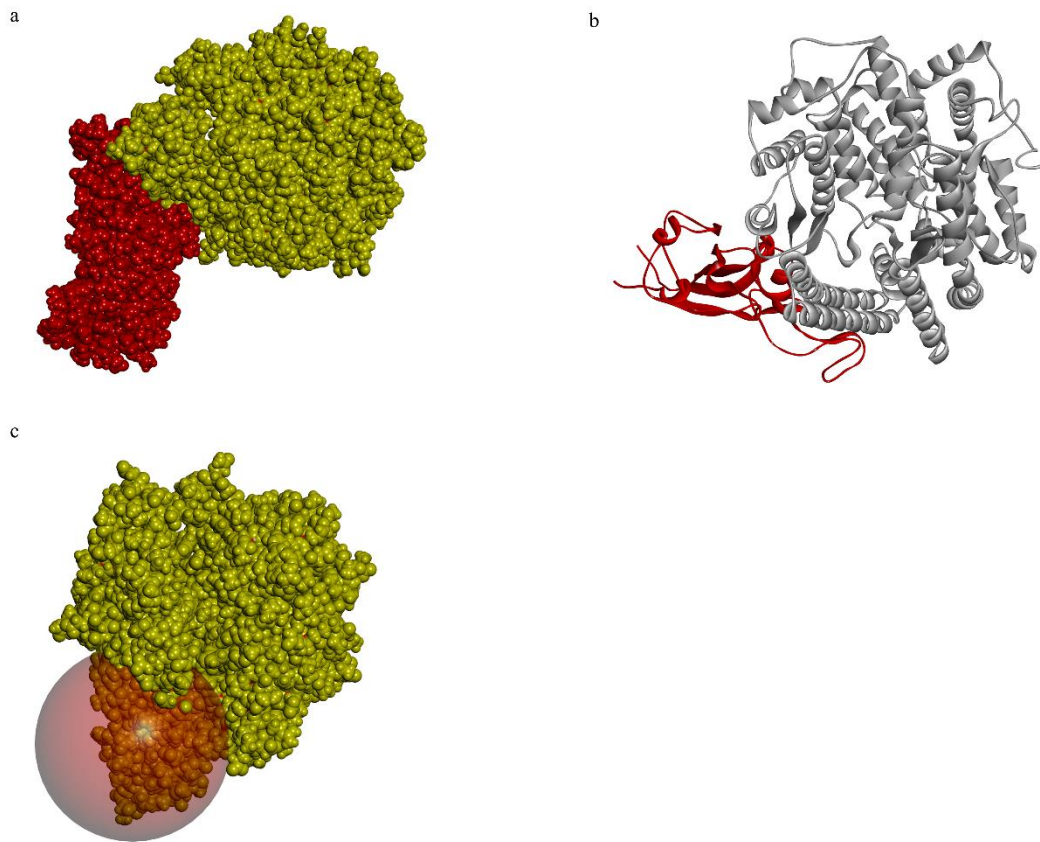


Fig. 6. a) Surface representation ACE-2: RBD of SARS-CoV-2 spike protein complex ACE-2. ACE-2 receptor protein is in yellow colour and RBD of SARS-CoV-2 is in red colour. b) Cartoon representation of ACE-2: RBD of SARS-CoV-2 spike protein complex. ACE-2 receptor protein is in yellow colour and RBD of SARS-CoV-2 is in red colour. c) Prepared active site of ACE-2.

3.1.2. Structure of 3CL^{pro} receptor protein preparation

The previously resolved X-ray crystallography of SARS-CoV-2 3CL^{pro} at a high resolution of 2.16 Å was obtained from PDB (PDB ID 6LU7) in complex with the N3 inhibitor (ID PRD_002214) (Fig. 7a). The total structure weight was 34.4 kDa. The N3 inhibitor was bound to the present structure by conventional hydrogen bonds with PHE140, GLY143, HIS164, GLU166, GLN189, THR189 residues, carbon-hydrogen bonds with ASN142, Met165, HIS172, and Alkyl bonds with HIS41, MET49, LEU167, PRO168, and ALA191 (Fig. 7b, 7c, and 7d). The radius of the prepared binding site sphere was 13.82 Å and HIS41, MET49, PHE140, ASN142, GLY143, HIS164, MET165, GLU166, LEU167, PRO168, HIS 172, GLN189, THR190, and ALA191 (Fig. 3e). The prepared 3CL^{pro} was superimposed with the original 3CL^{pro} available in PDB PyMOL and the calculated RMSD value was 0.185.

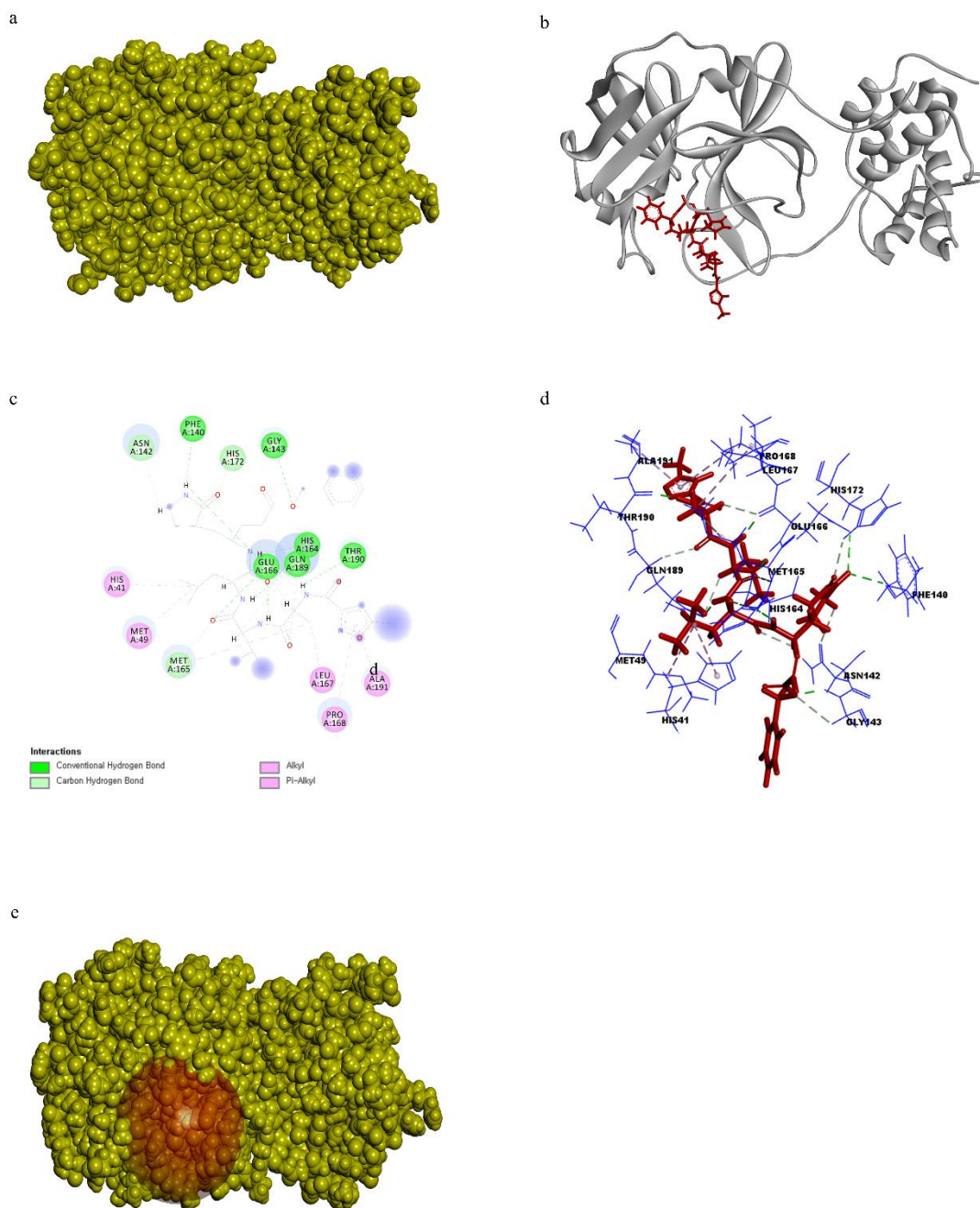


Fig. 7. a) Surface representation 3CL^{PRO} and N3 inhibitor ligand complex 3CL^{PRO} receptor protein is in yellow color and N3 inhibitor in red color. b) Cartoon representation of 3CL^{PRO} and N3 inhibitor ligand complex. 3CL^{PRO} receptor protein is in yellow color and N3 inhibitor is in red color. c) 2D representation of ligand interaction between 3CL^{PRO} and N3 inhibitor. d) 3D representation of ligand interaction between 3CL^{PRO} and N3 inhibitor. e) Prepared active site of 3CL^{PRO}.

3.1.3 Structure of PL^{pro} receptor protein preparation

The previously resolved X-ray crystallography of SARS-CoV-2 3CL^{pro} at a high resolution of 2.16 Å was obtained from PDB (PDB ID 6LU7) in complex with the N3 inhibitor (ID PRD_002214) (Fig. 8a). The total structure weight was 34.4kDa. The N3 inhibitor was bound to the present structure by conventional hydrogen bonds with PHE140, GLY143, HIS164, GLU166, GLN189, THR189 residues, carbon-hydrogen bonds with ASN142, Met165, HIS172, and Alkyl bonds with HIS41, MET49, LEU167, PRO168, and ALA191 (Fig. 8b, 8c, and 8d). The radius of the prepared binding site sphere was 13.82 Å and HIS41, MET49, PHE140, ASN142, GLY143, HIS164, MET165, GLU166, LEU167, PRO168, HIS 172, GLN189, THR190, and ALA191 (Fig. 8e). The prepared 3CL^{pro} was superimposed with the original 3CL^{pro} available in PDB PyMOL and the calculated RMSD value was 0.185.

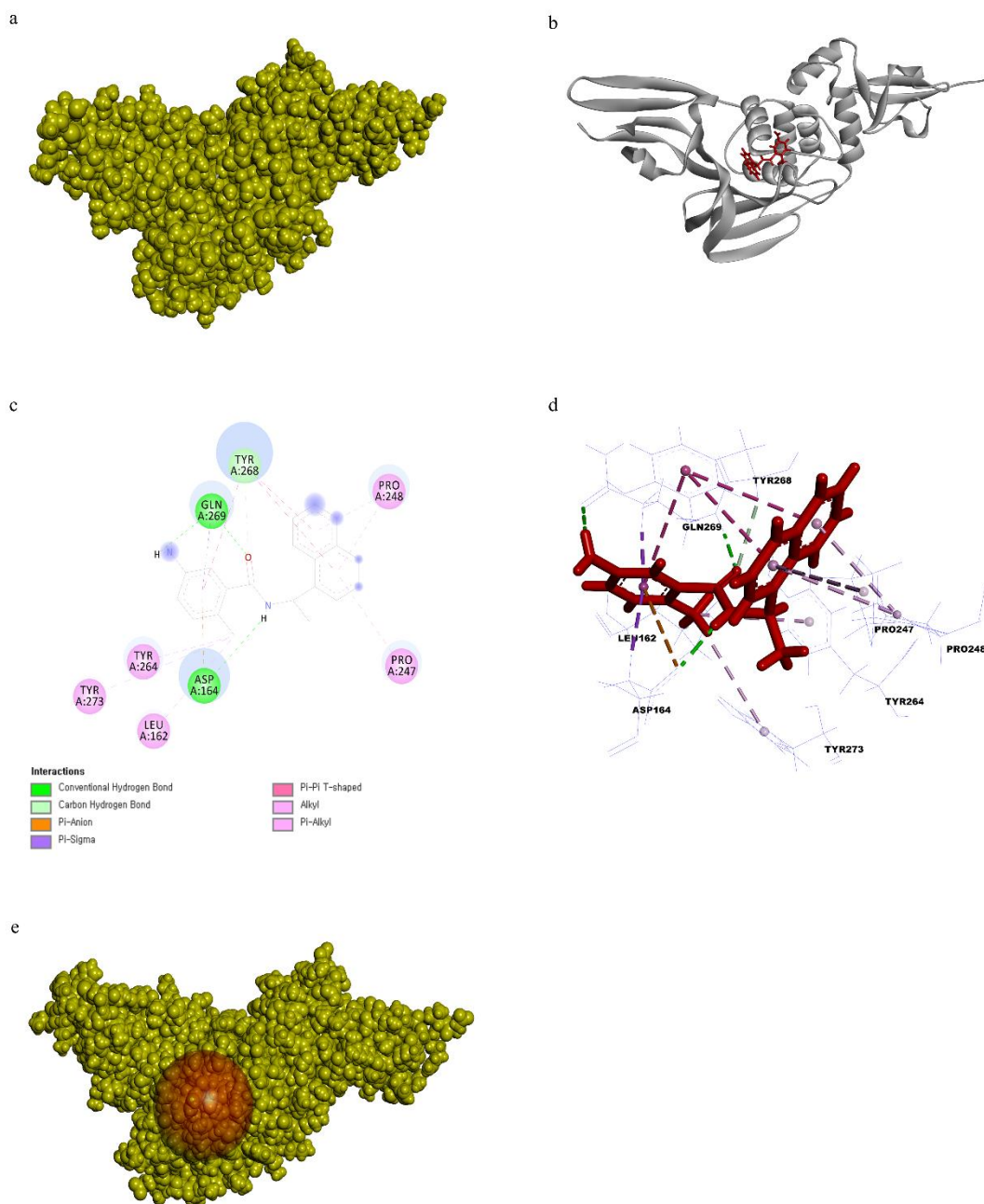


Fig. 8. a) Surface representation PL^{pro} and GRL0617 inhibitor ligand complex 3CL^{pro} receptor protein is in yellow color and GRL0617 inhibitor in red color. b) Cartoon representation of PL^{pro} and GRL0617 inhibitor ligand complex. PL^{pro} receptor protein is in yellow color and GRL0617 inhibitor is in red color. c) 2D representation of ligand interaction between PL^{pro} and GRL0617 inhibitor. d) 3D representation of ligand interaction between PL^{pro} and GRL0617 inhibitor. e) Prepared active site of PL^{pro}.

3.1.4 Ligand preparation

Total 16 ligands were prepared using DS “Prepare ligand” and all the prepared ligand structures were summarized in (Fig. 9). The most stable ligand conformation was used for molecular docking.

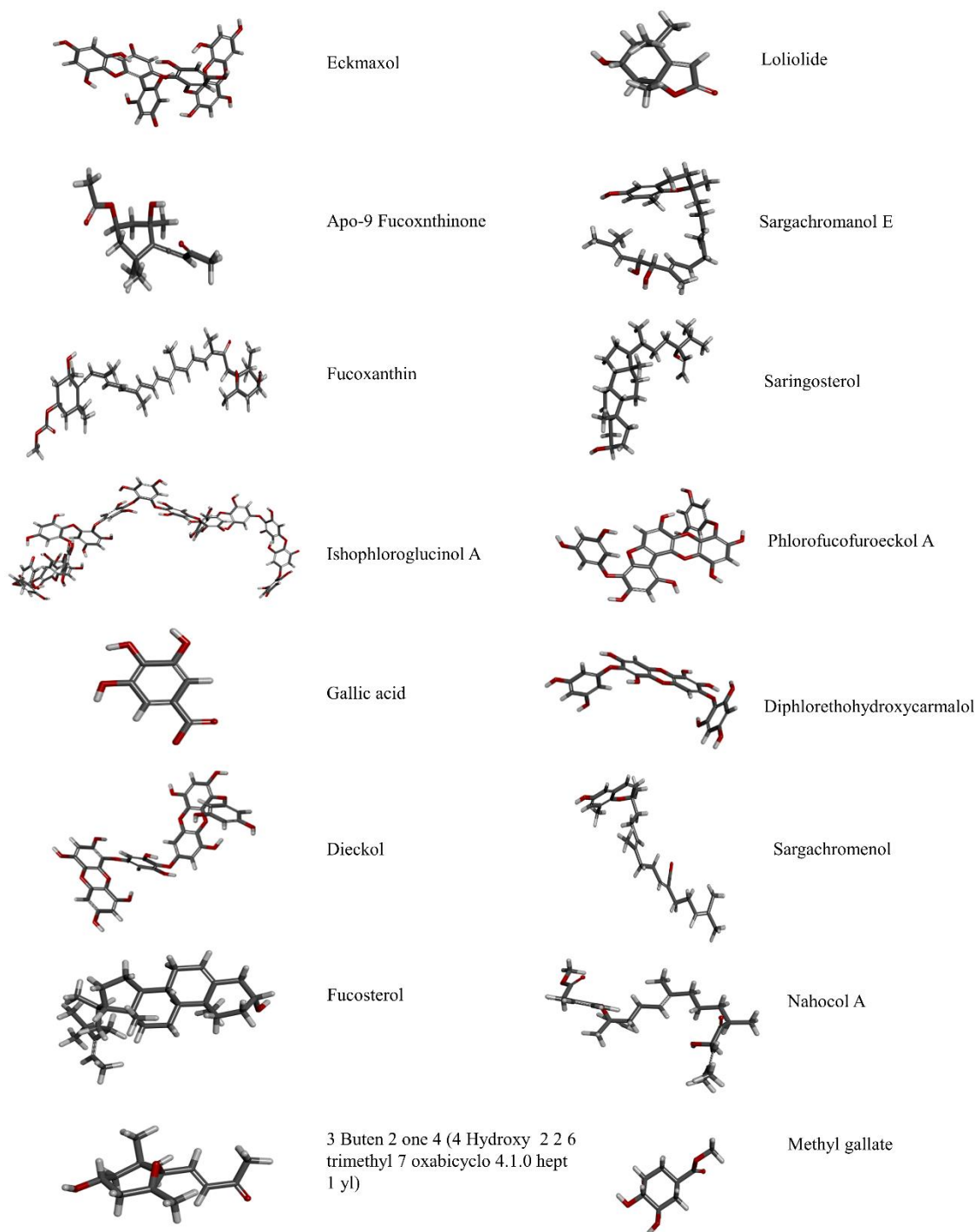


Fig. 9. Three-dimensional structures of prepared ligand using Discovery studio.

3.2 Molecular docking

Molecular docking was performed between all ligands and ACE-2, 3CL^{pro}, and PL^{pro} receptor proteins separately. The corresponding dock scores are summarized in Table 1, Table 2, and Table 3 respectively. According to the flexible docking, binding energy results, and DS visualizer results, Ishophloroglucin A (IPA), Dieckol, and Eckmaxol were selected for further studies.

Table 1. The cDock interaction energies and free binding energies (kcal/ mol) of selected ligands from marine algae with ACE-2 receptor protein.

No	Sample name	cDock interaction energy (kcal/ mol)	Binding energy (kcal/ mol)
1	Ishophloroglucinol A	-33.3206	-336.334
2	Diphlorethohydroxycarmalol	-114.898	-161.514
3	Dieckol	-44.5389	-78.6144
4	Phlorofucofureckol-A	-36.2067	-146.96
5	Nahocol A	-50.1917	-97.2917
6	Saringosterol	-35.8752	-66.8693
7	Sargacromanol E	-49.5546	-94.6006
8	Fucoxanthin	-	-
9	Eckmaxol	-68.572	-257.705
10	Fucosterol	-32.6457	-83.1795
11	Gallic acid	-16.4961	60.5235
12	Methyl gallate	-24.6816	-63.4524
13	Apo-9 fucoxanthinone	-	-
14	3-Buten-2-one,4-(4-hydroxy-2,2,6-trimethyl-7-oxabicyclo[4.1.0]hept-1-yl)-	-32.5717	-40.7664
15	Loliolide	-30.4983	-72.4829
16	Sargachromenol	-41.4074	-108.13

Table 2. The cDock interaction energies and free binding energies (kcal/ mol) of selected ligands from marine algae with 3CL^{pro} receptor protein.

No	Sample name	cDock interaction energy (kcal/ mol)	Binding energy (kcal/ mol)
1	GC376	-58.7189	-182.685
2	N3 inhibitor	-72.5369	-185.054
3	Ishophloroglucinol A	-63.1128	-186.875
4	Diphlorethohydroxycarmalol	-63.1128	-158.462
5	Dieckol	-68.0895	-257.388
6	Phlorofucofureckol-A	-	-
7	Nahocol A	-48.4205	-119.254
8	Saringosterol	-51.1228	-100.977
9	Sargacromanol E	-54.4594	-118.902
10	Fucoxanthin	-	-
11	Eckmaxol	-7.9218	-235.86
12	Fucosterol	-51.7309	-93.9243
13	Gallic acid	-28.1739	-141.556
14	Methyl gallate	-39.1007	-98.995
15	Apo-9 fucoxanthinone	-	-
16	3-Buten-2-one,4-(4-hydroxy-2,2,6-trimethyl-7-oxabicyclo[4.1.0]hept-1-yl)-	-27.7698	-62.684
17	Loliolide	-21.163	-93.869
18	Sargachromenol	-64.3135	-91.963

Table 3. The cDock interaction energies and free binding energies (kcal/ mol) of selected ligands from marine algae with PL^{pro} receptor protein.

No	Sample name	cDock interaction energy (kcal/ mol)	Binding energy (kcal/ mol)
1	GRL0617	-74.2579	-133.288
2	Ishophloroglucinol A	-43.5452	-271.055
3	Diphlorethohydroxycarmalol	-114.898	-146.253
4	Dieckol	-65.5972	-191.131
5	Phlorofucofuroeckol-A	-74.2645	-110.355
6	Nahocol A	-44.5236	-110.496
7	Saringosterol	-41.3209	-77.7694
8	Sargacromanol E	-54.1180	-15.2530
9	Fucoxanthin	-	-
10	Eckmaxol	-72.3064	-169.8830
11	Fucosterol	-34.7463	-71.5172
12	Gallic acid	-31.6026	-63.3519
13	Methyl gallate	-35.2097	-35.6745
14	Apo-9 fucoxanthinone	-	-
15	3-Buten-2-one,4-(4-hydroxy-2,2,6-trimethyl-7-oxabicyclo[4.1.0]hept-1-yl)-	-33.9821	-74.9392
16	Loliolide	-21.1630	-93.8690
17	Sargachromenol	-47.2003	-115.477

3.2.1. ACE-2 enzyme

IPA was stabilized with ACE-2 receptor via one conventional hydrogen bond through ARG393 with 2.28 Å length and one pi-pi stacked bond through ALA386 with 5.10 Å length. Furthermore, there are another two salt bridges that can be found between APA and HIS34 residue of ACE-2 with 1.78 Å and 5.99 Å length (Fig. 10).

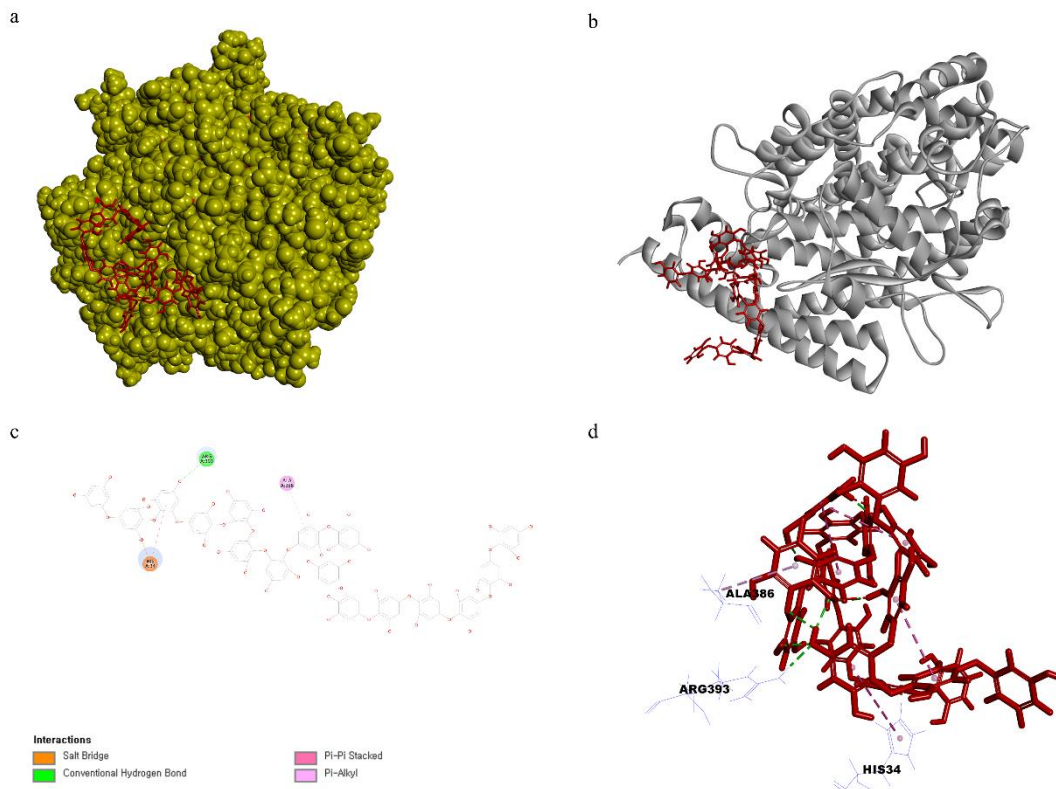


Fig. 10. a) 3D representation of docking pose of IPA with ACE-2. b) Cartoon representation of docking pose of IPA with ACE-2. c) 2D representation of Ligand interaction of IPA with ACE-2. d) 3D representation of Ligand interaction of IPA with ACE-2.

Eckmaxol was bound to the ACE-2 via three conventional hydrogen bonds through ASN397, ASP206, and GLY205 residues with 2.04 Å, 1.97 Å, and 1.97 Å length respectively. In addition, there is one pi-donor hydrogen bond with ASN394 residue, and the bond length was 2.60 Å length. ALA99 residue of ACE-2 made a pi-alkyl bond with Eckmaxol 4.33 Å length. LYS562 residue made a salt bridge with Eckmaxol and the length of the bond was 4.33 Å (Fig. 11).

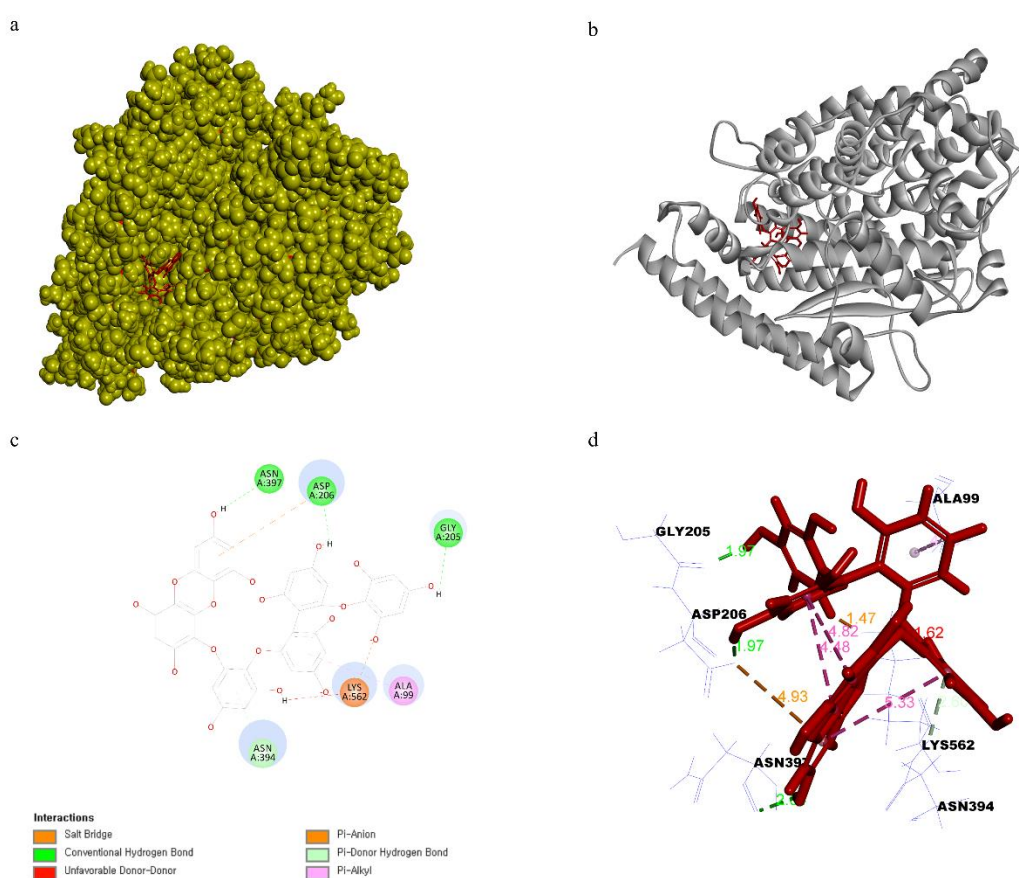


Fig. 11. a) 3D representation of docking pose of Eckmaxol with ACE-2. b) Cartoon representation of docking pose of Eckmaxol with ACE-2. c) 2D representation of Ligand interaction of Eckmaxol with ACE-2. d) 3D representation of Ligand interaction of Eckmaxol with ACE-2.

3.2.2. 3CL^{PRO} enzyme

IPA was bound to the binding site of 3CL^{PRO} through THR26, ASN119, PHE140, ASN142, GLY143, PRO168, and THR190 residues via conventional hydrogen bonds with the length of 2.35 Å, 2.30 Å, 1.92 Å, 1.99 Å, 2.93 Å, 2.96 Å, 2.31 Å respectively and GLU166 made 3 hydrogen bonds with 1.94 Å, 1.97 Å, and 1.94 Å length. Further, there is a 5.08 Å length one pi-sulfur bond with MET49 and 5.43 Å length pi-alkyl bond with LEU141(Fig. 12).

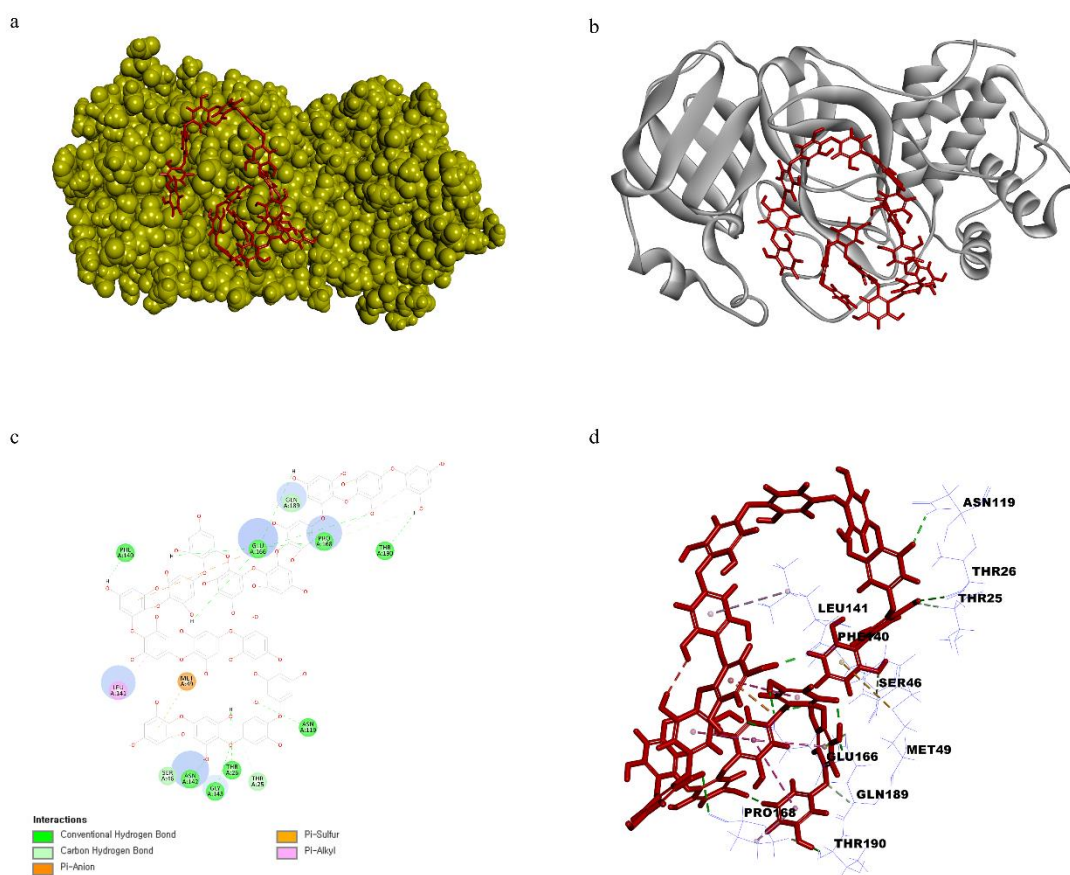


Fig. 12. a) 3D representation of docking pose of IPA with 3CL^{PRO}. b) Cartoon representation of docking pose of IPA with 3CL^{PRO}. c) 2D representation of Ligand interaction of IPA with 3CL^{PRO}. d) 3D representation of Ligand interaction of IPA with 3CL^{PRO}.

Dieckol was bound to the 3CL^{PRO} through four conventional hydrogen bonds with PHE140, ASN142, GLU166, PRO168, ARG188 and the length of bonds were 2.91 Å, 2.88 Å, 3.97 Å, 2.01 Å, and 2.21 Å respectively. Further, there are three pi-pi T-shaped bonds with HIS41, LEU141, HIS164 residues, and the length of each bond was 6.87 Å, 4.19 Å 5.33 Å respectively, and 4 pi-anion bonds. Among these bonds, binding take place between 5.28 Å length to CYS145, 5.33 Å length to HIS164, 4.41 Å length to MET165, and 5.64 Å, 5.22 Å length to with GLU166 residue, and finally, two pi-alkyl bonds with MET165 residue. The length of each bond was 4.67 Å and 5.09 Å (Fig. 13).

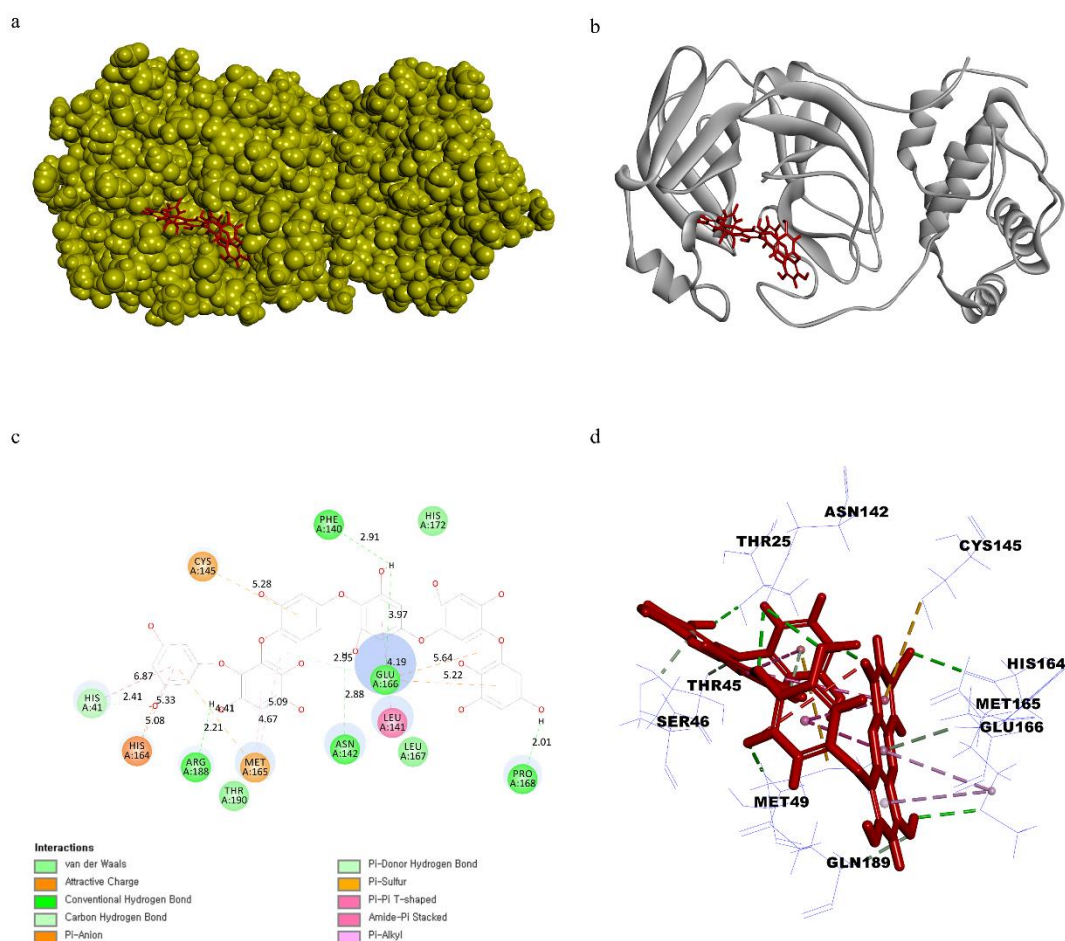


Fig. 13. a) 3D representation of docking pose of Dieckol with 3CL^{PRO}. b) Cartoon representation of docking pose of Dieckol with 3CL^{PRO}. c) 2D representation of Ligand interaction of Dieckol with 3CL^{PRO}. d) 3D representation of Ligand interaction of Dieckol with 3CL^{PRO}.

Eckmaxol was bound to the 3CL^{PRO} using ASN142, GLY143, SER144, HIS164, GLU166, ASP187, GLN189 residues via conventional hydrogen bonds with 2.34 Å, 1.78 Å, 4.17 Å, 2.09 Å, 2.82 Å, 2.10 Å, 1.88 Å length respectively. Further, there are 4 carbon-hydrogen bonds PHE140, LEU141, MET165, LEU167 with 2.47 Å, 2.58 Å, 2.7 Å length respectively and two pi-alkyl bonds with MET49 and CYS145 residues with 4.62 Å and 4.77 Å length (Fig. 14).

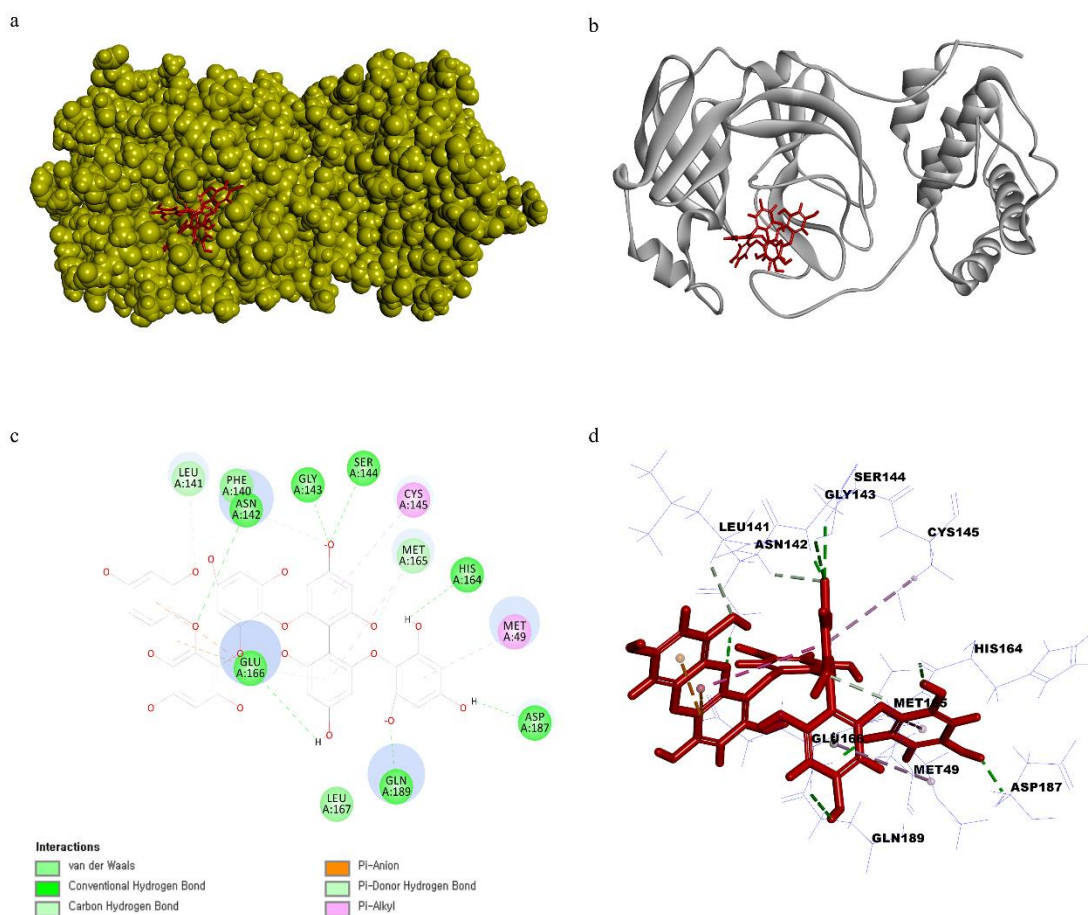


Fig. 14. a) 3D representation of docking pose of Eckmaxol with 3CL^{PRO}. b) Cartoon representation of docking pose of Eckmaxol with 3CL^{PRO}. c) 2D representation of Ligand interaction of Eckmaxol with 3CL^{PRO}. d) 3D representation of Ligand interaction of Eckmaxol with 3CL^{PRO}.

3.2.3. PL^{PRO} enzyme

IPA was bound to the PL^{PRO} by six conventional hydrogen bonds through ASP164, GLN250, TYR267, and TYR273 with 2.33 Å, 1.86 Å, 1.91 Å, and 1.91 Å length respectively. IPA made two conventional hydrogen bonds through ASN267 with 2.24 Å and 2.44 Å length. Furthermore, there are three pi-alkyl bonds between IPA and PL^{PRO} through PRO247 and ALA249 with 4.69 Å, 5.33 Å, 4.88 Å length and one pi-sulphur bond with MET208 residue with the length of 5.98 Å and one pi-anion bond through ASP164 with 3.24 Å length (Fig. 15).

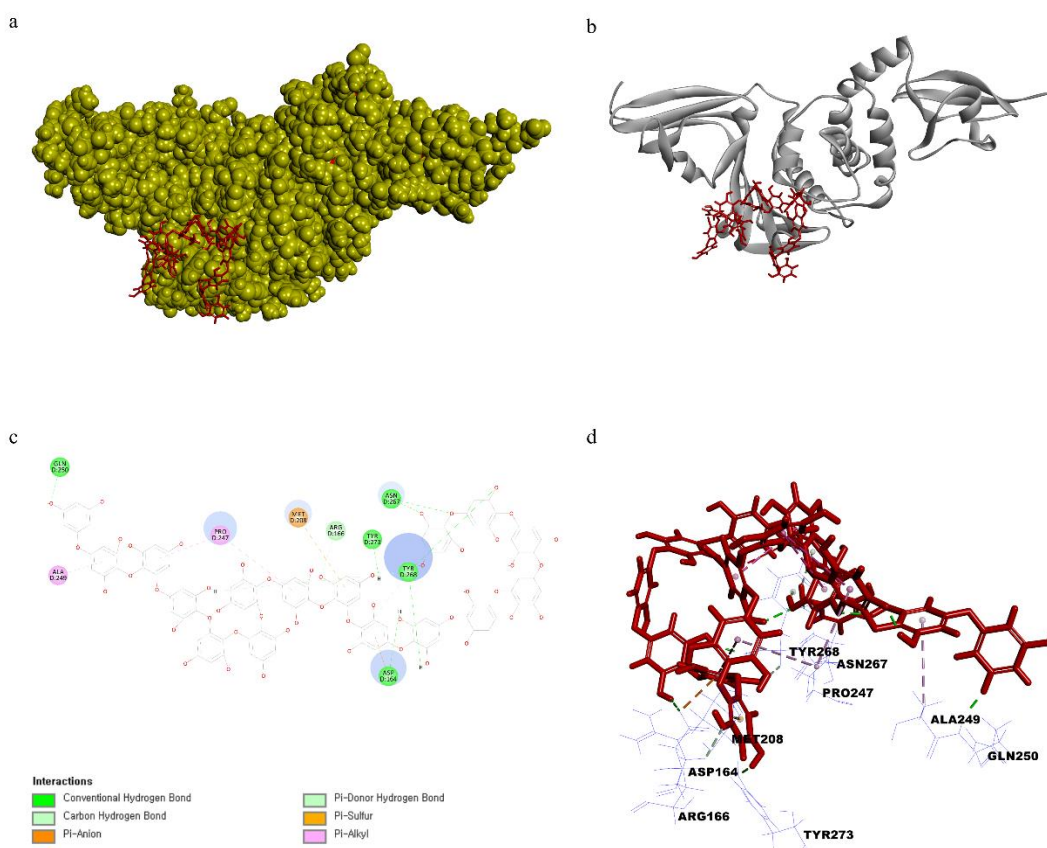


Fig. 15. a) 3D representation of docking pose of IPA with PL^{PRO}. b) Cartoon representation of docking pose of IPA with PL^{PRO}. c) 2D representation of Ligand interaction of IPA with PL^{PRO}. d) 3D representation of Ligand interaction of IPA with PL^{PRO}.

Dieckol made 3 conventional hydrogen bonds with PL^{PRO} through GLY163, TYR273, and THR302 residues and bond lengths were 1.91 Å, 2.18 Å, 2.06 Å. Further, PRO247 and SER245 made a carbon-hydrogen bond with 2.51 Å and 2.54 Å length. Moreover, PRO2478 made a pi-alkyl bond with 5.50 Å length. ARG166 made a salt bridge with 1.75 Å length and ASP164 bind to Dieckol via three pi-anion with 4.87 Å, 4.0 Å, and 3.90 Å. ALA246 made two amide-pi stacked bonds with 5.50 Å and 5.37 Å length. THR301 residue made a 2.88 Å length pi-lone pair with Dieckol. (Fig. 16).

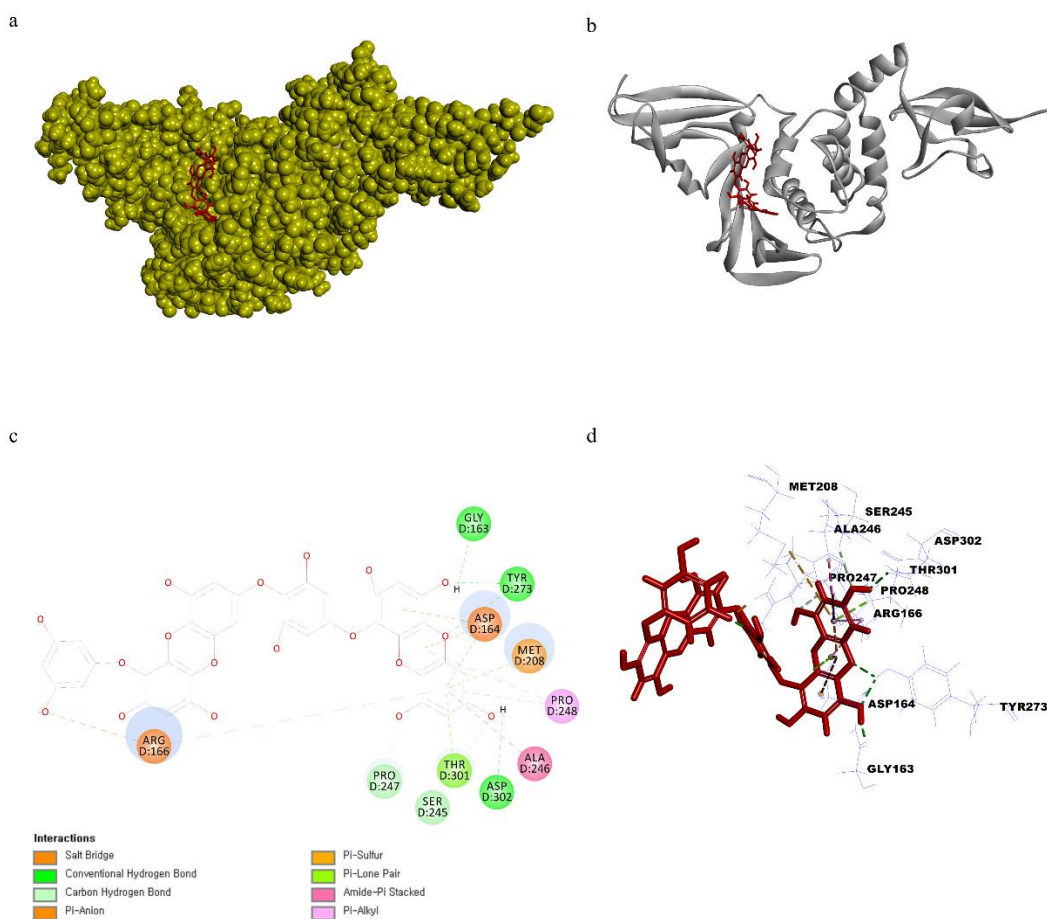


Fig. 16. a) 3D representation of docking pose of Dieckol with PL^{PRO}. b) Cartoon representation of docking pose of Dieckol with PL^{PRO}. c) 2D representation of Ligand interaction of Dieckol with PL^{PRO}. d) 3D representation of Ligand interaction of Dieckol with PL^{PRO}.

Eckmaxol was bound to the PL^{PRO} through ARG166, TYR273, and ASP302 residues via conventional hydrogen bonds with 2.01 Å, 2.41 Å, and 2.76 Å length respectively. Further, there are two carbon-hydrogen bonds between Eckmaxol and PRO248 and TYR248 with 2.62 Å and 2.91 Å length respectively. PRO247 made two pi-alkyl bonds with Eckmaxol with 5.00 Å, 4.98 Å length, and POR248, ARG166 made another pi-alkyl bond with 5.36 Å and 5.43 Å length respectively (Fig. 17).

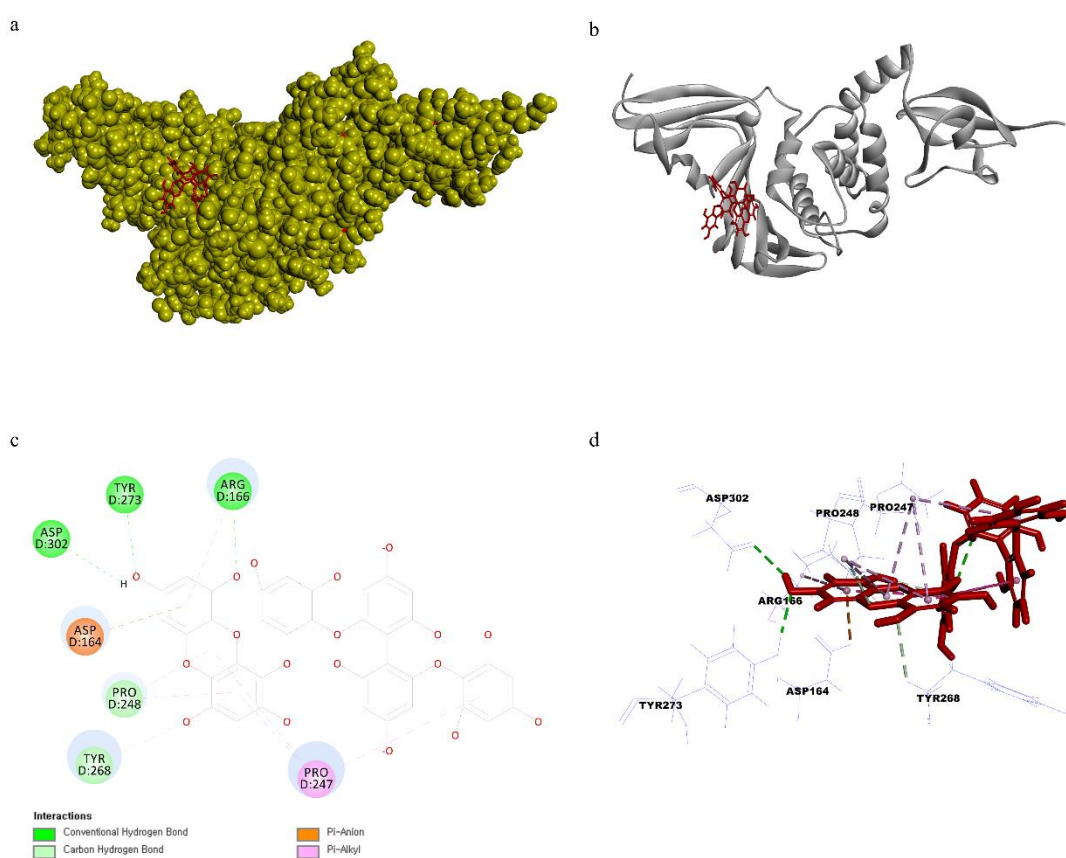


Fig. 17. a) 3D representation of docking pose of Eckmaxol with PL^{PRO}. b) Cartoon representation of docking pose of Eckmaxol with PL^{PRO}. c) 2D representation of Ligand interaction of Eckmaxol with PL^{PRO}. d) 3D representation of Ligand interaction of Eckmaxol with PL^{PRO}.

3.3 In-vitro inhibition of marine algal compounds

The inhibition ability of IPA, Dieckol, and Eckmaxol was evaluated using an in-vitro inhibition assay kit of 3CL^{pro} and PL^{pro}. The results are summarized in Table 4. The inhibition of cell entry mechanism of SARS-CoV-2 through ACE-2 receptor was evaluated using the ACE-2: SARS-CoV-2 RBD binding inhibition assay kit. IPA and Eckmaxol significantly downregulated the binding between ACE-2 and SARS-CoV-2 (Fig. 18). As shown in results, IPA expressed remarkable dose-dependent inhibition activity against 3CL^{pro}. Moreover, Dieckol and Eckmaxol showed elevated inhibition activity (Fig. 19). PL^{pro} cleavage mechanism also inhibited by IPA with lowest IC₅₀ value. Dieckol and Eckmaxol also inhibited the mechanism of PL^{pro} significantly (Fig. 20).

Table 4. Inhibitory activity of isolated compounds on the cell free cleavage of 3CL^{pro}, PL^{pro} and interactions of ACE-2: SARS-CoV-2 spike protein.

No	Drug target	Ligand	IC ₅₀ value (μM)
1	ACE-2	Ishophloroglucin A	115.77 ± 0.39
2		Eckmaxol	339.95 ± 0.67
3	3CL ^{pro}	Ishophloroglucin A	0.43 ± 0.031
4		Dieckol	5.48 ± 0.44
5		Eckmaxol	1.91 ± 0.078
6	PL ^{pro}	Ishophloroglucin A	1.41 ± 0.042
7		Dieckol	19.40 ± 0.82
8		Eckmaxol	27.25 ± 0.93

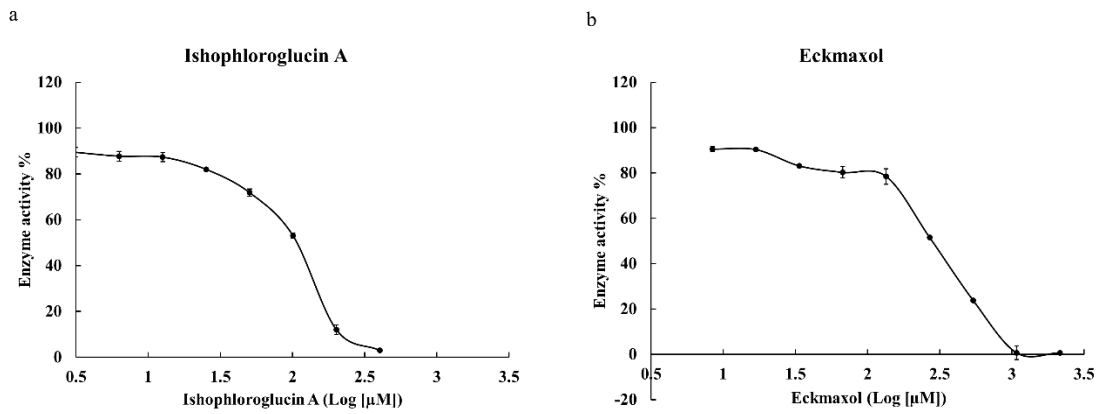


Fig. 19. *In-vitro* inhibition assay of the interaction between ACE-2: SARS-CoV-2 a) Ishophloroglucin A and b) Eckmaxol.

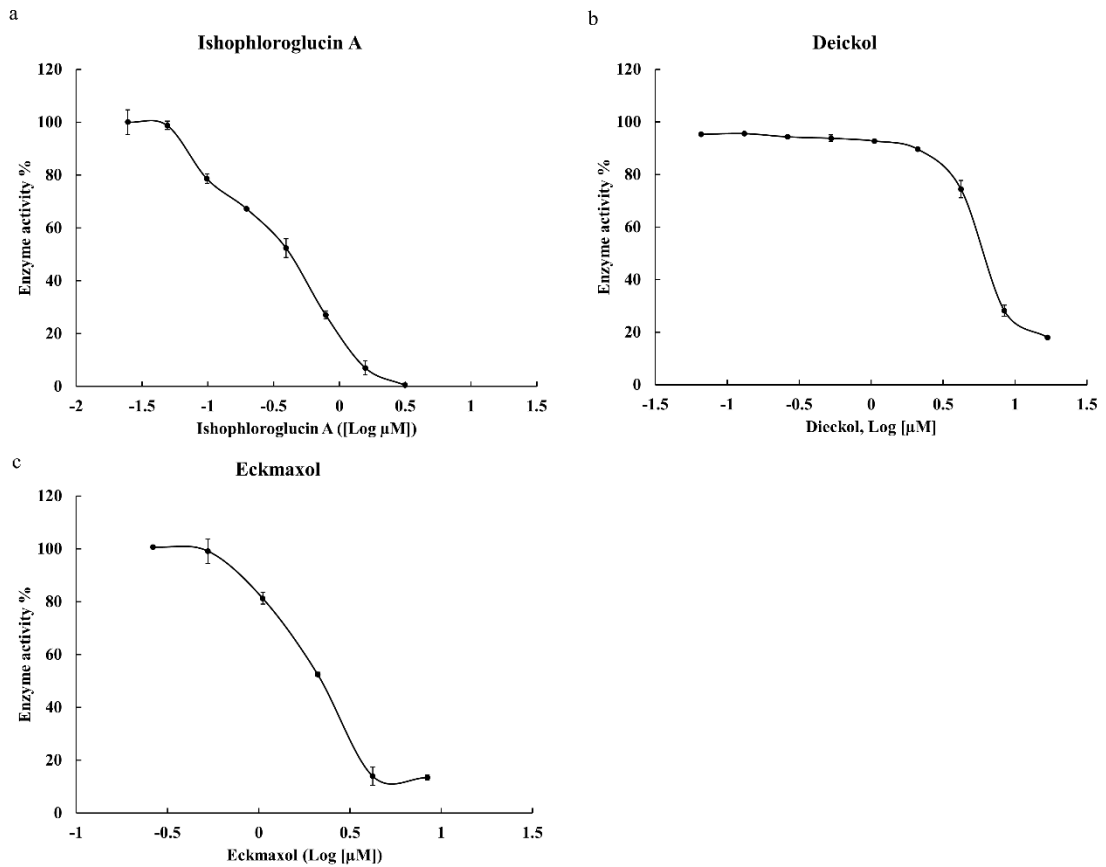


Fig. 18. *In-vitro* inhibition assay of 3CL^{pro} a) Ishophloroglucin A and b) Dieckol, and c) Eckmaxol.

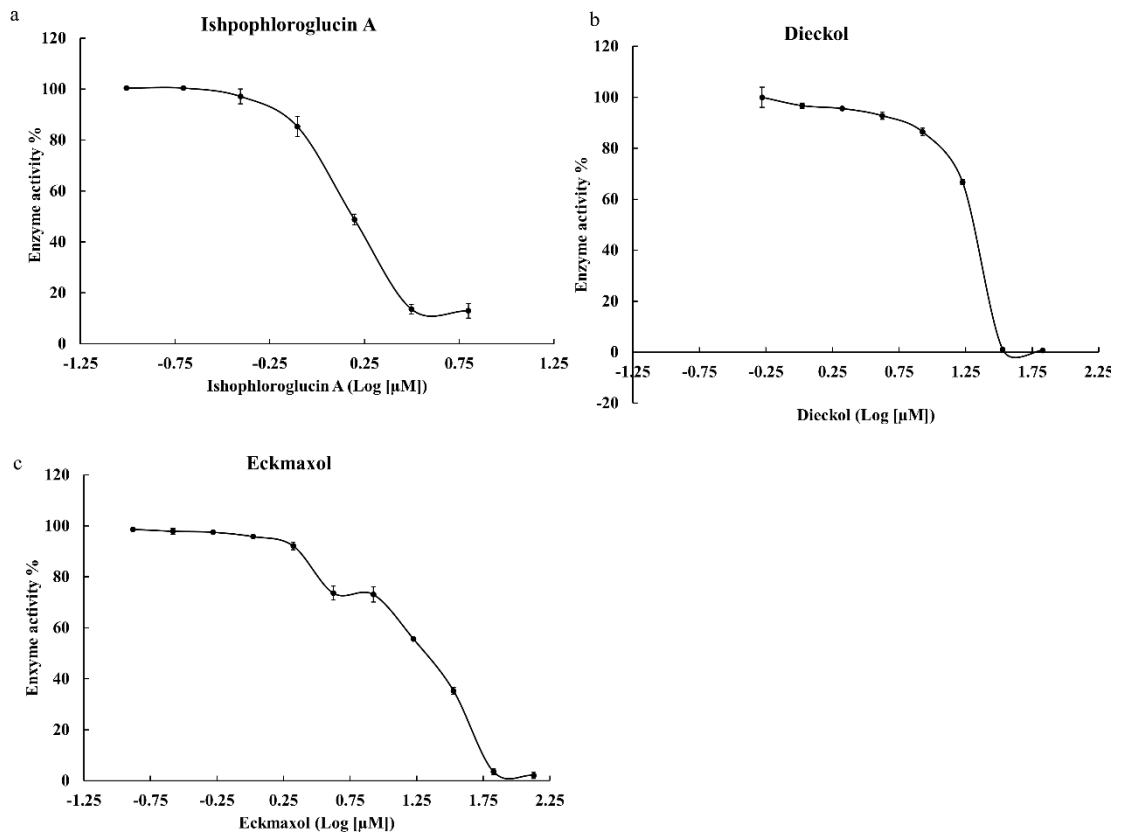


Fig. 20. In-vitro inhibition assay of PL^{pro} a) Ishophloroglucin A, b) Dieckol, and c) Eckmaxol.

4. Discussion

A lot of viruses employ numerous receptors and/or co-receptors for penetrating into host cells [31]. Receptor recognition by coronavirus is the first and essential step for entering human cells. The spike protein of coronaviruses is defined as one of the biggest viral spike glycoproteins known, so it is plausible to imagine that different domains within a single spike protein could interact with various receptors rendering easier and faster the entry of the virus. This aspect is crucial because, while it is ascertained that ACE-2 is the most recognized door for the entry, on the other side to target only ACE-2 could be limiting considering that recent data shows ACE-2 is up-regulated in diabetes and treatment with ACE inhibitors and angiotensin II Type-I receptor blockers [32]. Therefore, it would mean that an increased expression of ACE-2 would be associated to an easier infection with SARS-CoV-2. Therefore, this aspect suggests that a COVID-19 therapy by a multi-targeting approach is the right way. In this work, *in-silico* approach using docking studies has been performed for initial screening of the compounds based on the binding energy of ligands with ACE-2, 3CL^{pro} and PL^{pro}.

ACE-2 is a single pass type 1 membrane monocarboxypeptidase, discovered 2 decades ago [33]. ACE-2 consists of a N-terminal peptidase domain and C-terminal collecting like domain. It is the peptidase domain that is responsible for the main functions of the renin angiotensin system (RAS). The ACE-2 shares 40% homology with the N-terminal catalytic domain of ACE, and a hydrophobic region near the C-terminus likely to serve as a membrane anchor [34]. The ACE-2 protein is encoded by the ACE-2 gene located on chromosome Xp22. These ACE-2 proteins are more abundantly expressed on the apical surface of the well-differentiated and mostly ciliated airway epithelium of the lungs (alveolar Type-2 cells), and enterocytes of the small intestine [35]. Furthermore,

ACE-2 protein is expressed in arterial and venous endothelial cells and arterial smooth muscle cells, in the heart, kidneys, adrenal glands, pancreas, skeletal muscle, and adipose tissues [33]. The coronavirus SARS-CoV-2, has been seen to infect humans through their spike protein which is responsible for CoV cell entry and host-to-host transmission. During viral infection, this spike protein cleaves into S1 and S2 sites [34]. The FURIN cleavage site in the SARS-CoV-2 spike protein may provide a priming mechanism [36]. The ectodomain S1 of spike protein binds to the peptidase domain of the ACE-2 enzyme, while the S2 is cleaved further by the host cell serine protease TMPRSS2 resulting in membrane fusion. Both of these steps are essential for the viral entry into the cells [37]. An *in vivo* study shows that the infection of human airway epithelia by SARS coronavirus correlated with the state of cell differentiation and ACE-2 expression and localization. The infection tends to occur more readily through well differentiated ciliated cells with higher ACE-2 expression [38]. Therefore, the present study evaluated the inhibitory activity of IPA, Dieckol and Eckmaxol on ACE-2: SARS-CoV-2 spike protein binding. IPA bound to the ACE-2 receptor protein via conventional hydrogen bond with ARG393 residue. The bond length was 2.28°A. Moreover, it was stabilized on ACE-2 by another pi-pi stacked bond with ALA386 (5.10°A) and two salt bridges HIS34 residue (1.78°A and 5.99°A). The molecular docking results revealed that IPA shielded ACE-2 from RBD of spike protein. This result was further confirmed by *in-vitro* assay. IPA successfully inhibited the ACE-2: spike protein binding. These results suggested IPA as a potential drug candidate against SARS-CoV-2. Eckmaxol also significantly downregulated the ACE-2: spike protein binding and expressed the potential as an inhibitor to SARS-CoV-2 cell entry mechanism.

Among the excellent drug targets of SARS-CoV-2 are its proteases 3CL^{pro} playing vital

role in polyprotein processing giving rise to functional nonstructural proteins, essential for viral replication and survival [39]. The present study made an attempt to identify druggable sites in 3CL^{pro} and also investigated the binding interactions between 3CL^{pro} and marine natural products. As revealed from docking and simulation results, top hit compounds, IPA, Dieckol and Eckmaxol revealed stable binding with the active site of 3CL^{pro}. The molecular docking results were expressed that IPA was stable with 3CL^{pro} 7 conventional hydrogen bonds. The length of bonds was varying between 1.96 – 2.96 °A. The number of hydrogen bond also plays a critical role in determining the strength of the interaction. More the number of hydrogen bond having lesser bond length results in better binding [40]. Moreover, IPA made several types of bonds with 3CL^{pro} and provide an elevated inhibition ability against 3CL^{pro} dependent polyprotein processing. The inhibition activity of Dieckol and Eckmaxol was solidified by molecular docking and *in-vitro* assay results.

PL^{pro} plays a key role in polyprotein processing with 3CL^{pro}. PL^{pro} suppresses innate immunity through reversing the ubiquitination and ISGylation events. Therefore, Drugs that target SARS-CoV-2 PL^{pro} may hence be effective as treatments or prophylaxis for COVID-19, reducing viral load and reinstating innate immune responses. A common mechanism by which viral proteases regulate innate immune pathways is through antagonizing ubiquitin and ubiquitin-like modification [41]. Inflammatory signaling pathways rely on distinct ubiquitin signals that are regulated by intricate mechanisms in human cells [42]. ISG15 is an ubiquitin-like (Ubl) modification induced upon viral infection [43]. . ISG15 itself comprises two Ubl folds that are fused, structurally resembling diubiquitin [44]. Only few cellular enzymes remove ISG15, enabling this modification to act as a virus-induced danger signal. Importantly, coronaviral PL^{pro} enzymes efficiently remove ISG15 and ubiquitin modifications, dampening

inflammation and anti-viral signaling [45]. Thus, the inhibition of PL^{pro} activity takes an important role in SARS-CoV-2 inhibition. IPA binds to the active site of PL^{pro} mainly using 6 conventional hydrogen bonds and the length of bonds was between 1.86- 2.44°A. Further, PL^{pro} utilize several types of bonds for stabilization. *In-vitro* results suggested the binding ability of IPA with PL^{pro} and the applicability as an inhibitor against SARS-CoV-2 PL^{pro}. Dieckol and Eckmaxol also showed interesting inhibition activity against PL^{pro}. The overall results suggested the applicability of IPA, Dieckol and Eckmaxol as a potent inhibitor against SARS-CoV-2.

5. Conclusions

In this study, we report for the first time that the potential of polyphenolic compounds isolated from brown marine algae as an inhibitor against SARS-CoV-2 through main three drug target. The inhibition activities of isolated compounds against 3CL^{pro} PL^{pro}, and ACE-2: RBD of SARS-CoV-2 spike protein were assessed with molecular docking and *in-vitro* biological assay. From these results, IPA was identified as a most potent drug candidate against SARS-CoV-2.

Acknowledgment

I would like to express my gratitude and honour to my supervisor Professor Jeon You-Jin, Head, Marine Bio-Resource Technology Lab, Department of Marine Life Sciences, Jeju National University. His expertise was vital in the formulation of the research, his consistent guidance steered me through the right direction. I'm grateful to Professor Jeon for allowing me to conduct my own work and the opportunity created for me at his laboratory.

I would also like to single out Dr. Asanka Sanjeewa, who introduced me to Professor Jeon and Mr. Thilina U. Jayawardena whom he is my long-term colleague. Assistant, Associate Professors, post-doctoral positions, and all the lab mates are unforgettably mentioned with their dearest support towards my stay and work in the lab environment.

Finally, I must express my profound gratitude to my family for providing me with unflinching support throughout my years of study. This would have not been accomplished without them.

Though I have not pin pointed with names all the people who helped me, they are remembered and my gratitude is extended to them.

D.P. Nagahawatta

References

1. Zhou, P., et al., *A pneumonia outbreak associated with a new coronavirus of probable bat origin*. Nature, 2020. **579**(7798): p. 270-273.
2. Huang, C., et al., *Clinical features of patients infected with 2019 novel coronavirus in Wuhan, China*. The Lancet, 2020. **395**(10223): p. 497-506.
3. Organization, W.H., *Summary of probable SARS cases with onset of illness from 1 November 2002 to 31 July 2003*. http://www.who.int/csr/sars/country/table2004_04_21/en/index.html, 2003.
4. De Wit, E., et al., *SARS and MERS: recent insights into emerging coronaviruses*. Nature Reviews Microbiology, 2016. **14**(8): p. 523.
5. Lau, S.K.P., et al., *Severe acute respiratory syndrome coronavirus-like virus in Chinese horseshoe bats*. Proceedings of the National Academy of Sciences of the United States of America, 2005. **102**(39): p. 14040.
6. Chan, J.F.-W., et al., *A familial cluster of pneumonia associated with the 2019 novel coronavirus indicating person-to-person transmission: a study of a family cluster*. The Lancet, 2020. **395**(10223): p. 514-523.
7. Rothan, H.A. and S.N. Byrareddy, *The epidemiology and pathogenesis of coronavirus disease (COVID-19) outbreak*. Journal of Autoimmunity, 2020. **109**: p. 102433.
8. Li, F., *Structure, Function, and Evolution of Coronavirus Spike Proteins*. Annual Review of Virology, 2016. **3**(1): p. 237-261.
9. Du, L., et al., *The spike protein of SARS-CoV — a target for vaccine and therapeutic development*. Nature Reviews Microbiology, 2009. **7**(3): p. 226-236.
10. Li, F., *Receptor Recognition Mechanisms of Coronaviruses: a Decade of Structural Studies*. Journal of Virology, 2015. **89**(4): p. 1954.
11. Li, F., et al., *Structure of SARS Coronavirus Spike Receptor-Binding Domain Complexed with Receptor*. Science, 2005. **309**(5742): p. 1864.
12. Li, F., *Structural Analysis of Major Species Barriers between Humans and Palm Civets for Severe Acute Respiratory Syndrome Coronavirus Infections*. Journal of Virology, 2008. **82**(14): p. 6984.
13. Wu, K., et al., *Mechanisms of Host Receptor Adaptation by Severe Acute Respiratory Syndrome Coronavirus*. Journal of Biological Chemistry, 2012. **287**(12): p. 8904-8911.
14. Hoffmann, M., et al., *SARS-CoV-2 Cell Entry Depends on ACE2 and TMPRSS2 and Is Blocked by a Clinically Proven Protease Inhibitor*. Cell, 2020. **181**(2): p. 271-280.e8.
15. Wan, Y., et al., *Receptor Recognition by the Novel Coronavirus from Wuhan: an Analysis Based on Decade-Long Structural Studies of SARS Coronavirus*. Journal of Virology, 2020. **94**(7): p. e00127-20.
16. Lu, R., et al., *Genomic characterisation and epidemiology of 2019 novel coronavirus: implications for virus origins and receptor binding*. The Lancet, 2020. **395**(10224): p. 565-574.
17. Naqvi, A.A.T., et al., *Insights into SARS-CoV-2 genome, structure, evolution, pathogenesis and therapies: Structural genomics approach*. Biochimica et Biophysica Acta (BBA) - Molecular Basis of Disease, 2020. **1866**(10): p. 165878.
18. Anand, K., et al., *Coronavirus Main Proteinase (3CL^{pro}) Structure: Basis for Design of Anti-SARS Drugs*. Science, 2003. **300**(5626): p. 1763.

19. Ghosh, A.K., et al., *Design and Synthesis of Peptidomimetic Severe Acute Respiratory Syndrome Chymotrypsin-like Protease Inhibitors*. Journal of Medicinal Chemistry, 2005. **48**(22): p. 6767-6771.
20. Kumar, V., et al., *Identification, synthesis and evaluation of SARS-CoV and MERS-CoV 3C-like protease inhibitors*. Bioorganic & Medicinal Chemistry, 2016. **24**(13): p. 3035-3042.
21. Pillaiyar, T., et al., *An Overview of Severe Acute Respiratory Syndrome–Coronavirus (SARS-CoV) 3CL Protease Inhibitors: Peptidomimetics and Small Molecule Chemotherapy*. Journal of Medicinal Chemistry, 2016. **59**(14): p. 6595-6628.
22. Shin, D., et al., *Papain-like protease regulates SARS-CoV-2 viral spread and innate immunity*. Nature, 2020.
23. Solan, M. and N. Whiteley, *Stressors in the Marine Environment: Physiological and ecological responses; societal implications*. 2016: Oxford University Press.
24. Mostafa, S.S., *Microalgal biotechnology: prospects and applications*. Plant Science, 2012. **12**: p. 276-314.
25. Jin, Z., et al., *Structure of Mpro from SARS-CoV-2 and discovery of its inhibitors*. Nature, 2020. **582**(7811): p. 289-293.
26. Gao, X., et al., *Crystal structure of SARS-CoV-2 papain-like protease*. Acta Pharmaceutica Sinica B, 2020.
27. Wang, Q., et al., *Structural and Functional Basis of SARS-CoV-2 Entry by Using Human ACE2*. Cell, 2020. **181**(4): p. 894-904.e9.
28. Ryu, B., et al., *Ishophloroglucin A, a novel phlorotannin for standardizing the anti- α -glucosidase activity of *Ishige okamurae**. Marine drugs, 2018. **16**(11): p. 436.
29. Zhou, X., et al., *Isolation and purification of a neuroprotective phlorotannin from the marine algae *Ecklonia maxima* by size exclusion and high-speed counter-current chromatography*. Marine Drugs, 2019. **17**(4): p. 212.
30. Li, X.-Q., et al., *COMPARISON OF INHIBITORY EFFECTS OF THE PROTON PUMP-INHIBITING DRUGS OMEPRAZOLE, ESOMEPRAZOLE, LANSOPRAZOLE, PANTOPRAZOLE, AND RABEPRAZOLE ON HUMAN CYTOCHROME P450 ACTIVITIES*. Drug Metabolism and Disposition, 2004. **32**(8): p. 821.
31. Jeffers, S.A., et al., *CD209L (L-SIGN) is a receptor for severe acute respiratory syndrome coronavirus*. Proceedings of the National Academy of Sciences of the United States of America, 2004. **101**(44): p. 15748.
32. Fang, L., G. Karakiulakis, and M. Roth, *Antihypertensive drugs and risk of COVID-19? - Authors' reply*. The Lancet. Respiratory medicine, 2020. **8**(5): p. e32-e33.
33. Donoghue, M., et al., *A Novel Angiotensin-Converting Enzyme-Related Carboxypeptidase (ACE2) Converts Angiotensin I to Angiotensin 1-9*. Circulation Research, 2000. **87**(5): p. e1-e9.
34. Yan, R., et al., *Structural basis for the recognition of SARS-CoV-2 by full-length human ACE2*. Science, 2020. **367**(6485): p. 1444-1448.
35. Hamming, I., et al., *Tissue distribution of ACE2 protein, the functional receptor for SARS coronavirus. A first step in understanding SARS pathogenesis*. The Journal of Pathology: A Journal of the Pathological Society of Great Britain and Ireland, 2004. **203**(2): p. 631-637.
36. Lukassen, S., et al., *SARS-CoV-2 receptor ACE2 and TMPRSS2 are predominantly expressed in a transient secretory cell type in subsegmental bronchial branches*. bioRxiv, 2020: p. 2020.03.13.991455.
37. Hoffmann, M., et al., *SARS-CoV-2 Cell Entry Depends on ACE2 and TMPRSS2 and Is Blocked by a Clinically Proven Protease Inhibitor*. Cell, 2020. **181**(2): p. 271-280 e8.

38. Jia, H.P., et al., *ACE2 Receptor Expression and Severe Acute Respiratory Syndrome Coronavirus Infection Depend on Differentiation of Human Airway Epithelia*. *Journal of Virology*, 2005. **79**(23): p. 14614.
39. Kumar, P., et al., *Reprofiling of approved drugs against SARS-CoV-2 main protease: an in-silico study*. *Journal of Biomolecular Structure and Dynamics*, 2020: p. 1-15.
40. Jeffrey, G., *An Introduction to Hydrogen Bonding: Oxford University Press: New York, 1997*. There is no corresponding record for this reference.[Google Scholar]: p. 220-225.
41. Isaacson, M.K. and H.L. Ploegh, *Ubiquitination, Ubiquitin-like Modifiers, and Deubiquitination in Viral Infection*. *Cell Host & Microbe*, 2009. **5**(6): p. 559-570.
42. Ebner, P., G.A. Versteeg, and F. Ikeda, *Ubiquitin enzymes in the regulation of immune responses*. *Critical Reviews in Biochemistry and Molecular Biology*, 2017. **52**(4): p. 425-460.
43. Perng, Y.-C. and D.J. Lenschow, *ISG15 in antiviral immunity and beyond*. *Nature Reviews Microbiology*, 2018. **16**(7): p. 423-439.
44. Dzimianski, J.V., et al., *ISG15: It's Complicated*. *Journal of Molecular Biology*, 2019. **431**(21): p. 4203-4216.
45. Harcourt, B.H., et al., *Identification of Severe Acute Respiratory Syndrome Coronavirus Replicase Products and Characterization of Papain-Like Protease Activity*. *Journal of Virology*, 2004. **78**(24): p. 13600-13612.